

出國報告（出國類別：參加研討會）

# 出席 2013 年國際能源應用材料會議 心得報告

服務機關：國防大學理工學院動力及系統工程學系

姓名職稱：王樂民教授

派赴國家：德國

出國期間：102/5/10~102/5/19

報告日期：102/6/6

## 摘要

國際研討會“材料於能源上的應用(International Conference on Materials for Energy)”乃國際間能源材料應用上知名會議，會議摘要歷經審查機制，獲接受論文必須收錄及供與會人士下載。

此會議參與學者遍及世界各國，學者研究範圍極廣，學術討論分為：能源效率、儲存、燃料電池、電化學儲存、鎳基超合金材料之應用、氫的儲存、材料應用環境、熱電學(Thermoelectrics)、能源效率、磁性材料材料製造程序及其模擬(Modeling)、生化燃料、光電材料、催化性能(Catalysis)、導電材料、固態照明(Solid-State lighting)、奈米材料應用在電極上、奈米材料應用在燃料電池、奈米材料應用於太陽能電池等 20 種議題，極為豐碩。

議程有 5 場專業大會報告，238 篇論文報告，本人發表“鈦合金經過儲氫/放氫後改進耐蝕性能”，此乃一新方法，參與學者積極提問，評價良好，此行除吸取新知外，經由與國外學者討論，獲益良多，有助於未來教學研究之精進。

## 目次

|                         |    |
|-------------------------|----|
| 摘要.....                 | 2  |
| 目次.....                 | 3  |
| 目的.....                 | 4  |
| 過程.....                 | 4  |
| 心得及建議.....              | 8  |
| 附件一：本人受邀發表論文簡報.....     | 9  |
| 附件二：會中發表及參與研討之論文.....   | 25 |
| 附件三：大會函文邀請本人提供簡報資料..... | 43 |

## 目的

- 1.赴德國研討會，發表研究成果。
- 2.與國際學者進行學術交流。

## 過程

此次研討會於 5 月 12-16 日假德國 Karlsruhe 市會議中心(Convention Center)舉行，計有大會演講論壇、論文報告及論文海報展示及說明等事項。

此次會議著重於能源儲存運用，以開發材料來達到改進材料及精進科技上之應用，並可望應用於嚴苛環境提昇。

5 月 12 日 1000-1800 時開始接受與會人員報到及論文海報展示備便，1800-2000 時為歡迎晚宴。5 月 13 日 1000-1030 時為大會開幕式，1030-1230 時由大會邀請之 M. Fleischer 教授就 Mesoscopic photosystems for the generation of electricity and fuels from sunlight 與 C. A. Volkert 教授就 Energy storage-challenges and perspectives 實施演講，當日 1230 時即開始依大會規劃之場地就各議題實施分組報告與意見交流，期間大會另於 5 月 15 日 0845-1215 時，安排 L. Schultz 教授就 Energy efficient transportation by superconducting levitation-riding on magnetic fields、J. DeYoreo 教授就 Recent developments in solar photovoltaics : market, industry, and technology 及 D. Aranda 教授就 Challenges in the microalgae energy feasibility 實施專題報告，最後大會於 5 月 16 日 1250 時舉行圓滿閉幕式。

經聽取大會安排之五位知名教授演講內容，汲取了目前國際間對於能源產出、儲存、傳遞及運用之市場需求觀點、技術發展近況及未來挑戰與願景，其中包含太陽光催化反應系統的技術開發；能源儲存之途徑與方式及其面臨之經濟效益、儲存效率及環境影響等相關工程技術挑戰；超導磁力懸浮之能源傳輸方式；以及國際間目前積極研究開發之藻類發電方式，經查國內台電公司目前亦投入發展微藻減碳計畫，規劃一套適合運用於火力發電廠的微藻養殖技術，利用電廠發電後所產生的煙氣及燃油集塵灰當作藻類生長所需的碳源及氮源，讓藻類在低耗能的養殖系統中轉化為大量的有機體以及氧氣。藻類經回收後，可將其中成分如多醣類、藻藍蛋白等活性物質萃取出來，再利用於機能食品、動物餌料或保養品等高經濟價值

產品的生產，而剩餘的藻體，可做為生物燃料（Biofuel），當作發電系統的燃料使用。

本人獲得邀請之論文口頭報告，大會安排於 5 月 14 日 1630-1650“Extreme Environment”議題中實施報告，由 Section, Prof .R. Moors 主持。演講主題為“以工業重要材料 Ti-6Al-4V 合金經熱置氫製程後，經由控制氧化層而提昇抗蝕性能之應用”（附件一）。此實驗方法乃新的研究方式，嘗試以 Ti-6Al-4V 合金經熱置氫製程長出之奈米晶粒後再實以熱處理，在奈米晶粒上生長出細薄氧化層，由於此方法乃創新研究，結合 Ti 合金易儲氫特性，並可改變材質之相變化。研究結果顯示此方法具體可行，其微觀結構及成型機制也被詳細了解，報告結束獲五人積極提問並獲滿意答覆。

其中所提問題概分為：

- (1)如何確認本人在儲放氫過程中，完全將氫吸收及排放。
- (2)Ti 合金理論上較不喜歡氫，易產生氫脆，儲氫效益難道不會受影響。
- (3)如果產生奈米晶粒，那麼機械性質表現如何？
- (4)如何量出吸氫量。
- (5)如何確定氫氣已全部排出，等 5 項。

針對上述 5 項提問，本人回答如下：

- (1)以 Sievert 's Volumetric Apparatus（投影片 8/31）之儀器進行熱置氫(THP)處理，此法已獲肯定，可以 THP Keywords 當關鍵字去搜尋 Scripta Mat.及 Acta Mat.等知名期刊當參考，可更了解細節。
- (2)此種技術以理想氣體方程式結合壓力閥的管制，壓力量測（8/31 投影片）可精確量出其儲放氫量，已屬成熟，不必質疑。
- (3)經過量測及觀察，本研究之硬度值均在  $H_v = 300$ ，是在  $\alpha$  相及  $\beta$  相內，繼續切割  $\alpha$  相及  $\beta$  相，而對外圍組織的大晶粒範圍，除了氧化層產生預期效果外，並無不良影響。否則以純粹奈米晶粒硬度，硬度就至少會達到  $H_v = 700-800$  以上。此種 THP 製程，效果極佳。
- (4)Ti 合金雖然與氫結合時易有氫脆，尤其是在固溶後+水淬。然而如果在儲氫時，Ti 極喜歡與氫原子接合。此特性才使得 Ti 合金有除氫功能，且可因此產生相變化，晶粒細化等有趣及值得應用的現象。避開水淬也是一種符合避免氫脆的產生。
- (5)以精確壓力的量測即可確定氫氣已排出。

事後更有美國南卡羅大學化工系教授 Prof. Jason Hattrick-Simpers 及蘇俄高階工程師（旅居德國），找本人繼續討論高解析影像的  $\alpha$ 、 $\beta$  相之奈米結構，進一步了解實驗細節。

個人於簡報後除聽取 5 月 15 日邀請報告外，並參與相關議題之參展海報交流(如附件二)，包含：

- Different types of cathode structures for lithium sulfur batteries.
- Study on the mechanism of lithium-ion battery by hyper branched polymer coated on cathode.
- Kinetics of acetic acid steam reforming over Ni/ and Co/Ce<sub>0.75</sub>Zr<sub>0.25</sub>O<sub>2</sub> catalysts.
- Casting process of CNTs-Al composites using composite powder precursors and intensive melt shear technology.
- Material development enabler formulation to turn active materials into finish products.
- Dual nitrogen and sulfur doped carbons as metal free catalysts for the oxygen reduction reaction in fuel cells.
- Structure, mechanical properties and conductivity of Cr and Hf Bronzes after ECAP.
- Nano-foams by continuity inversion of dispersion.
- High voltage core-shell nanocomposites as positive electrode materials for advanced lithium-ion batteries.
- Surface modification of carbons by elevated temperatures gas treatments for improved solid electrolytes interphase formation.
- In-situ stress evolution studies of (De) lithiated Si films.
- In situ and ex situ studies of lithium nucleation and dendritic growth during electroplating.
- XRD total scattering and pair distribution (PDF) measurements on LiNi<sub>0.5</sub>Mn<sub>1.5</sub>O<sub>4</sub> spinel.
- The EERA joint programme on energy storage.
- Nanoscale silicon as high capacity anode of next-generation lithium ion batteries.
- The influence of different carbon surfaces on electro-reduction of oxygen in different electrolytes.
- In-situ X-ray diffraction : time-resolved structure investigation of L-transition metal-fluorides as cathode materials in Li-ion batteries.
- The initial stage of lithium metal deposition studied by in situ STM.

由於大會配置識別證上有註記教授頭銜，因此在海報論文展示處，幾位學生自告奮勇邀

請本人至其海報論文前，希能給予其一些建議。本人聽其簡報後，針對電池極板材質改進後，亦給予 3 點改進意見，敘述如下：

- (1)效率提升須與較重要的現有文獻報告比較，查出其差異。
- (2)所提供的穿透式電子顯微鏡，雖然具有微細奈米顆粒影像，但無法證明是作者聲稱的粒子，必須輔之以 SADP 繞射圖形，證明其晶粒常數相符。必須要再多作上述實驗步驟或以高解析 TEM，以 FFT（快速傅立葉轉換）量出其聲稱的粒子繞射平面以證明。此二實驗可二選一，趕快補足，否則這篇論文若由我審查，我不會同意作者聲稱的結果，因為“嚴謹性不足”。
- (3)所提供之場發射照片雖然尚可，但本人認為仍需重拍攝，指出其未完美聚焦之處，使得影像更完美，以符合知名期刊之要求。

本人與上述學生互動良好，雙方留下深刻印象，並對國外投入大量人力及經費於能源材料研發精進印象深刻。

大會於會後並來函（[附件三](#)），希本人提供電子檔報告內容，並經由大會平台，提供與會人士下載繼續深入研究。

## 心得及建議

因能源危機的影響，為提升能源效率及因應材質性能提昇、減重、效能改進，以材料改善儲存方法及精進，乃今後科技發展之重心。今後將材料應用於嚴苛環境，其儲存方式、電池的性能提升、改進電池材料、燃料電池改進及太陽能電池應用等，為世界目前研究重點。

經過此次研討會深感科技之重要性，以及清楚看到過際間研發能量投入此領域，對其日後經濟強化，有重要影響。我國學人及業界應投入更多人力及經費，以免落後喪失國際間競爭舞台，可延伸國內的相關產業及研究方向，如提昇效率、對材料材質的改善、對機械性質的要求，以因應更為嚴格環境，如潛變的控制，材料機械性質維持也與能源同樣受到重視。

經歷此次研討會議，亦深覺教學研究責任重大，必本虛心以學習；看到國外學者最近研究成果，對材料材質改善量測技術、性能提升，不遺餘力，實值得我國相關科技人員深思及大力推展，以立足於世界競爭舞台，且深感英文能力表達及科技報告的閱讀能力之重要性，此後亦更加督促學生，使學生能與國際接軌更有競爭力。

附件一：本人受邀發表論文簡報

## Controlled Oxide Layer Formation on Corrosion Behavior of Ti-6Al-4V Alloy Following Thermohydrogen Processing

L. M. Wang, C. J. Tsai, S. L. Lee



Chung Cheng Institute of Technology,  
Dept. of Power Vehicle and System Engineering  
University of National Defense, Taiwan, R.O.C.



2<sup>nd</sup> International Conference on Materials for Energy



# Introduction

1. Ti-6-4 alloy is a promising material.

Major applications are in :

- aerospace,
- automobile,
- military industries

because of its :

- low density,
- excellent mechanical,
- corrosion properties

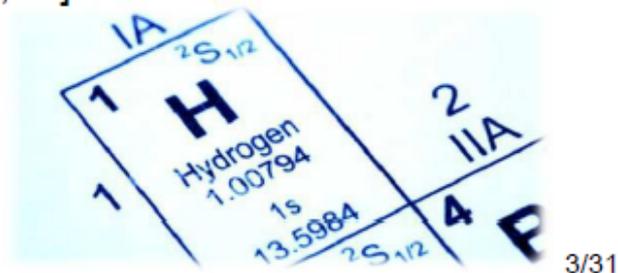


2/31

2. Recently, extensive studies have been reported on **refinement of the grain size** of titanium alloys using a **thermohydrogen process (THP)** by employing **hydrogen** as a **temporary alloying element**.

\*THP, by using :

**hydrogenation** and **dehydrogenation** process [Yu,06;She,07;She,09].



3. The **refinement** is achieved based on the

- **modifying effect of hydrogen**

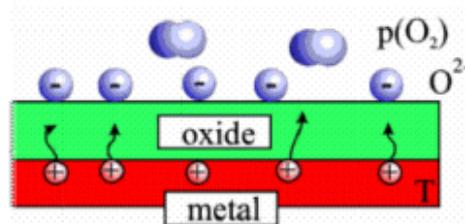
**on**

- **phase composition and transformation of metastable phases.**

4. Interestingly, even a relatively **low concentration** of **hydrogen** introduced into **titanium alloys** as a **temporary alloying element** has a **great effect** upon **phase transformation** and thus **modification of microstructure and mechanical properties** [Fro,04].

4/31

5. THP can produce **nano grains**.  
[Yu,06;She,07;She,09].
6. **Oxide layer** produced on nano grains may be a good way to enhance the **corrosion resistance** of Ti-6-4 alloy.
7. There are **limited reports** on the **corrosion behavior** of **grain-refined** Ti alloys resulting from the THP.



5/31

8. **Control of O<sub>2</sub> flowing rate** into the furnace containing THP processed sample of Ti-6-4 alloy may be possible to **control** the desirable **thickness** and **composition** of Ti-6-4 and therefore :  
improve the corrosion resistance of T-6-4 alloy.
9. So this study aims to evaluate whether this goal can be achieved.



6/31

# Experimental work

Sample preparation

- as-received(AR)
- $\beta$ -solution treatment at  $1050^{\circ}\text{C}$  in vacuum for 0.5 h, followed by furnace cooling to room temperature(AR+BST)

7/31

THP treatment

- Sievert's volumetric apparatus was used for THP treatment.
- Hydrogenation :  $600^{\circ}\text{C}/30\text{ min}$
- Dehydrogenation :  $600^{\circ}\text{C}/2\text{ h}$ , followed by air cooling for approximately 30 min to room temperature.

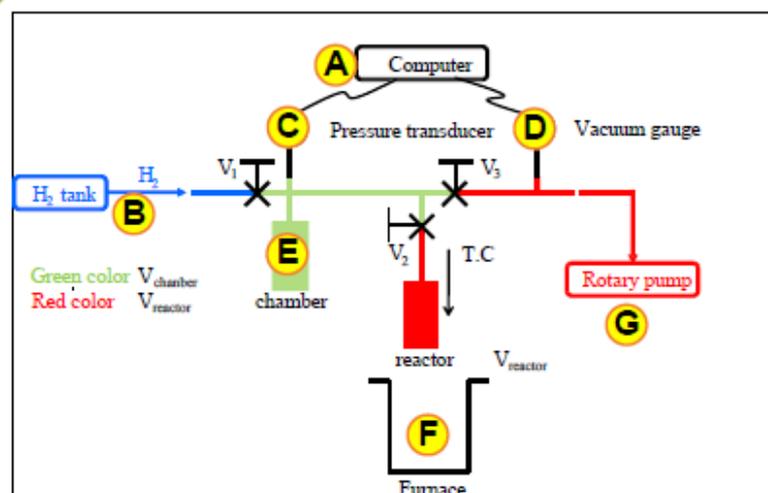
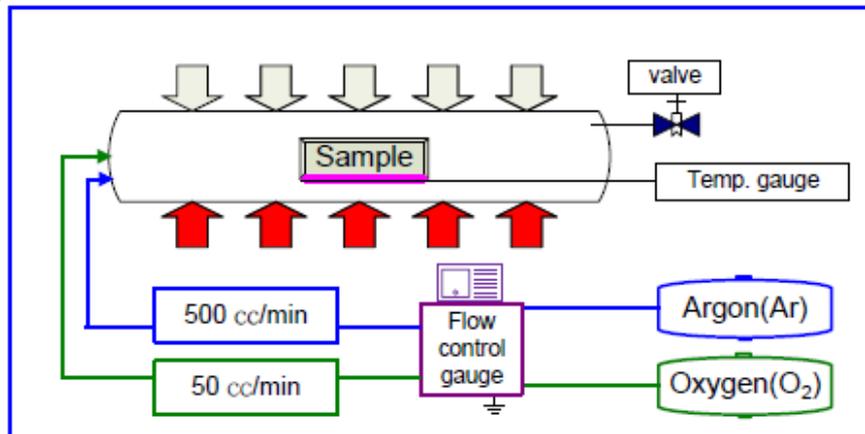


Fig.1 Sievert's volumetric apparatus diagram

8/31

Annealing treatment

- ANN : **without** O<sub>2</sub>+Ar (500cc/min) at 704°C/2h/air cooling
- ANN plus O<sub>2</sub> : **with** O<sub>2</sub>(50cc/min)+Ar (500cc/min) at 704°C/2h/air cooling



**Fig.2 Annealing treatment diagram**

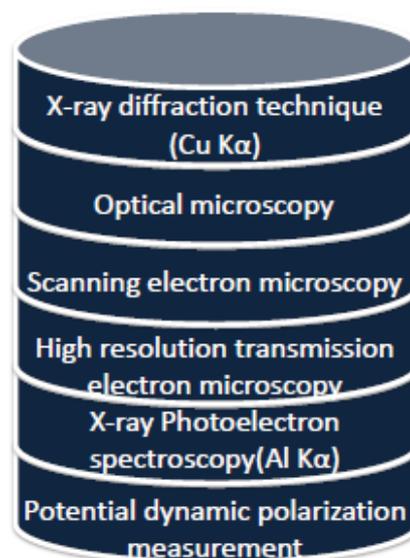
All the samples **were ground** with SiC abrasive papers and further polished with fine grade diamond paste before each stage treatment.

9/31

### Sample Condition

- A** AR+BST  
( $\beta$ -solution treatment)
- B** AR+BST+THP
- C** AR+BST+THP+ANN
- D** AR+BST+THP+ANN (O<sub>2</sub>)  
(50cc/min)
- E** AR+BST+ANN

### test



\*Sample A, B treated at vacuum condition.

\*Sample C, D, E prepared in argon filled atmosphere.

10/31

**TABLE I. Related processing and treatment of present samples**

| Sample   | Treatment Procedure   |
|--|---|
| AR+polished+BST* <sup>1</sup>                          | as-received → polished → $\beta$ solution treatment → exposing in air   |
| AR+BST+polished+THP* <sup>2</sup>                      | as-received → $\beta$ solution treatment → polished → thermohydrogen processing → exposing in air   |
| AR+BST+THP+polished+ANN* <sup>3</sup>                  | as-received → $\beta$ solution treatment → thermohydrogen processing → polished → annealing treatment → exposing in air   |
| AR+BST+THP+polished+ANN(O <sub>2</sub> )* <sup>4</sup> | as-received → $\beta$ solution treatment → thermohydrogen processing → polished → annealing treatment associated with oxygen flowing into the furnace (50 cc/min) → exposing in air |
| AR+BST+polished+ANN                                    | as-received → $\beta$ solution treatment → polished → annealing treatment → exposing in air   |

\*1. BST ( $\beta$  solution treatment): conducted in vacuum at 1000°C/30min/air cooling

2. THP (thermohydrogen processing): hydrogenated in vacuum at 600°C/30min → dehydrogenated in vacuum at 600°C/2h/air cooling

3. ANN (annealing treatment): carried out in furnace completely filled high purity argon at 704°C/2h/air cooling

4. ANN(O<sub>2</sub>): annealing treatment associated with controlled amount of oxygen flowing into the furnace at 50 cc/min

11/31

## Result and Discussion

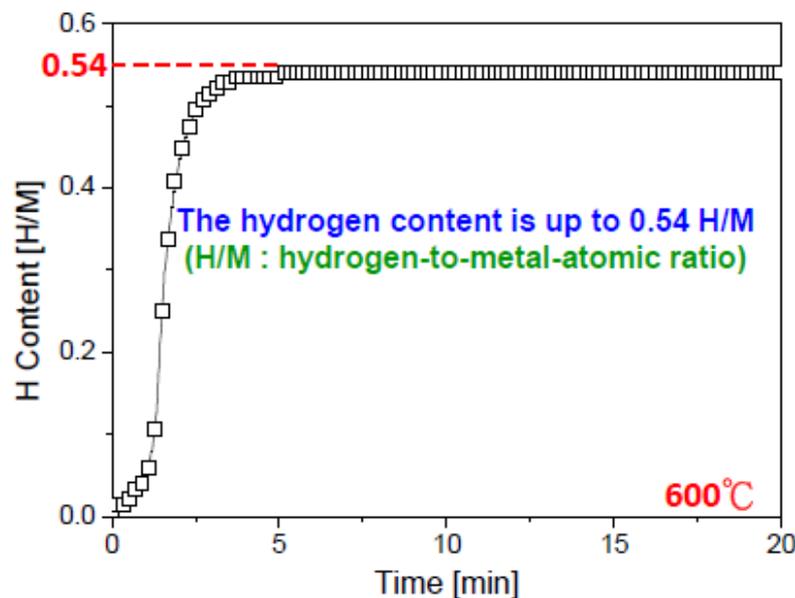


**Fig.3 Typical kinetic curves for hydrogen absorption**

12/32

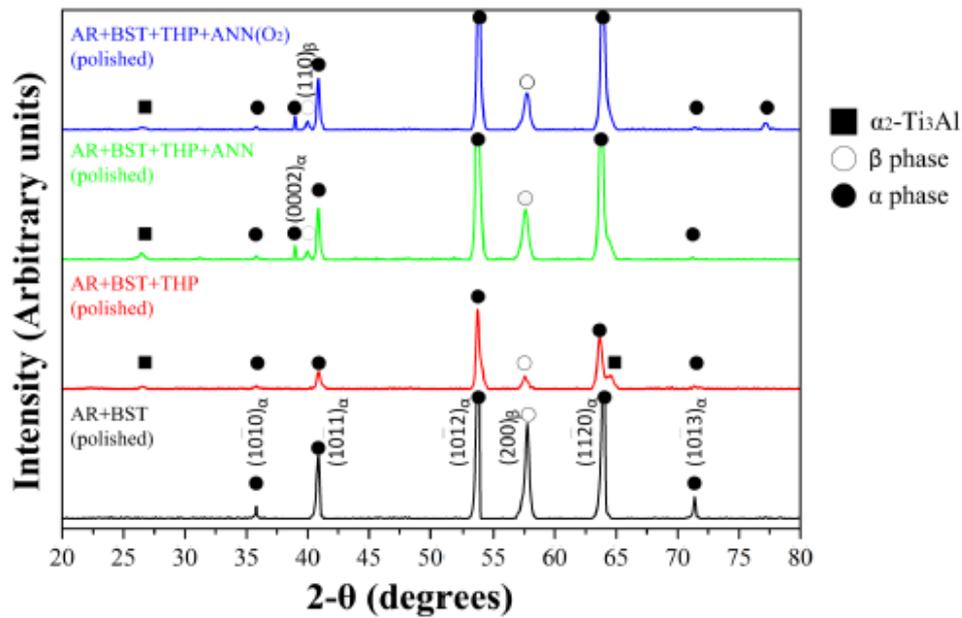


**Fig.4 XRD patterns of Ti-6-4 alloy after related treatments. The identified phases of  $\alpha$ ,  $\alpha_2$ , and  $\beta$  are marked.**

13/32

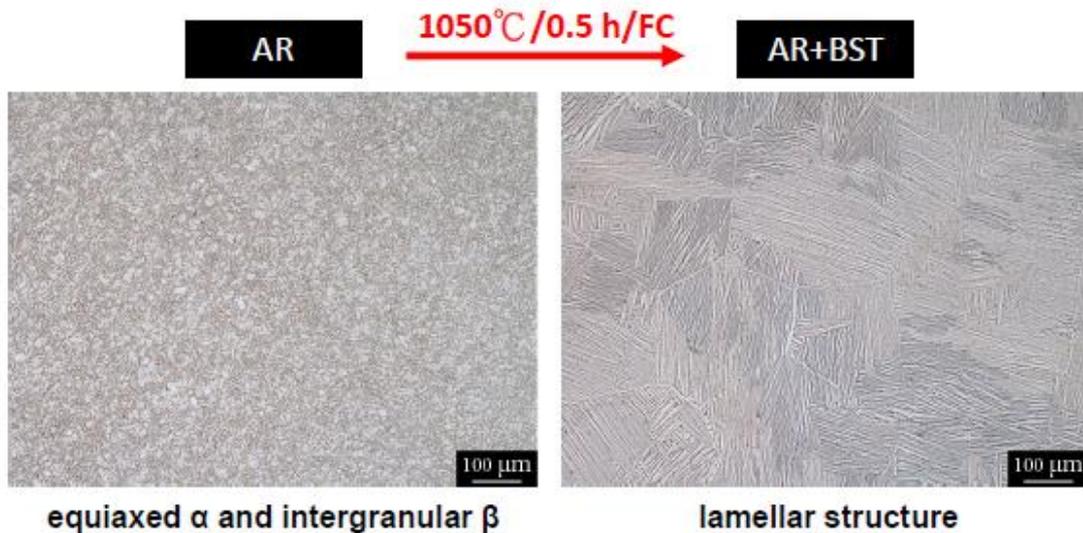


**Fig.5 Optical micrographs of  $\beta$ -solution treated Ti-6-4 alloy**

14/32

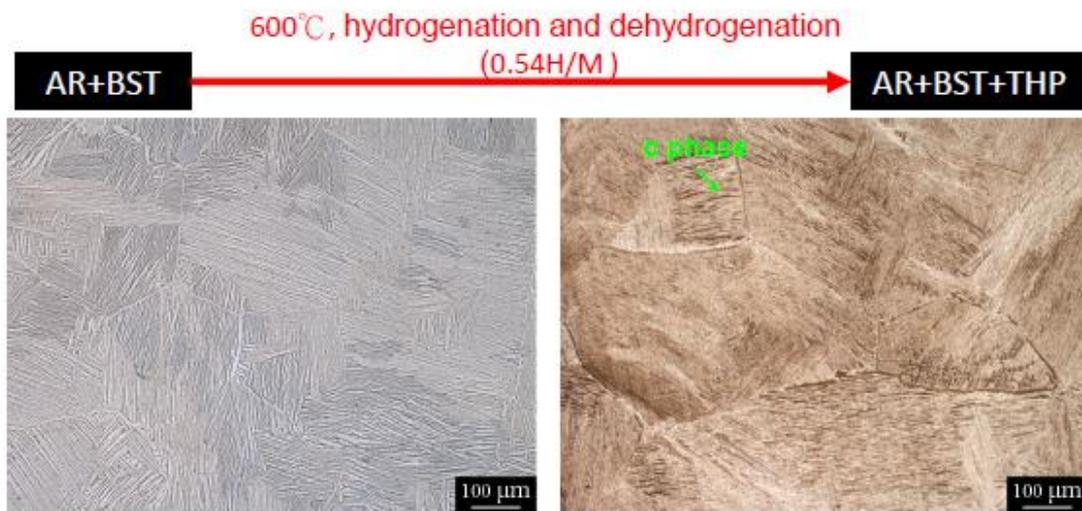


**Fig.6 Optical micrographs of Ti-6-4 alloy subjected to THP treatment at 600°C following  $\beta$ -solution treatment**

the lamellar structure is preserved  
associated with severely etched feature after THP treatment

15/32

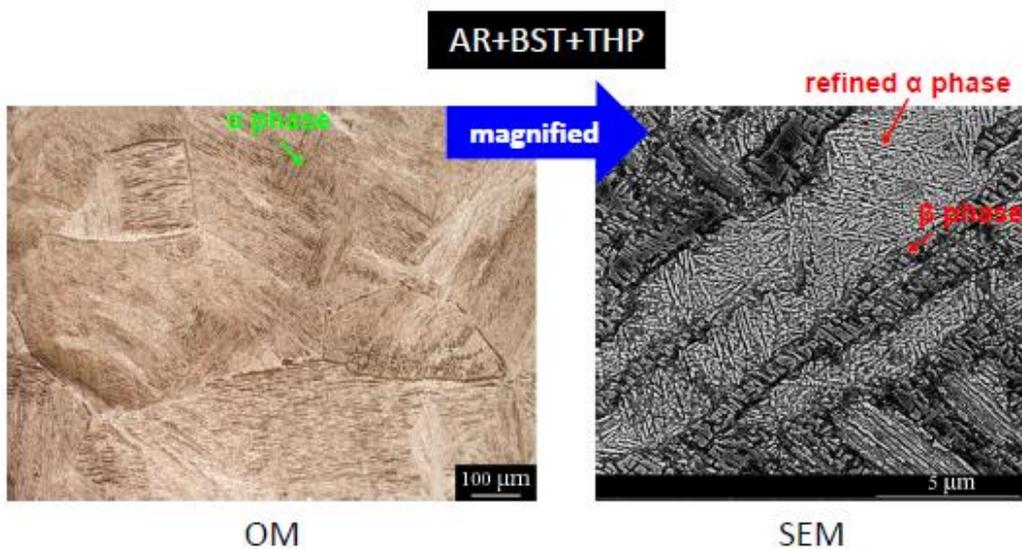
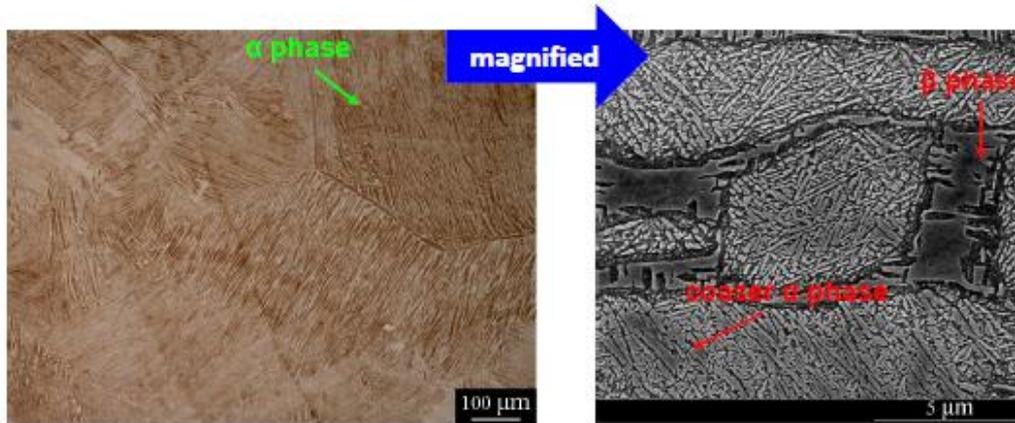


**Fig.7 Optical and SEM micrographs of Ti-6-4 alloy subjected to THP treatment at 600°C**

grain refinement within the  $\alpha$  matrix is observed  
through SEM technique

16/31

AR+BST+THP+ANN



OM

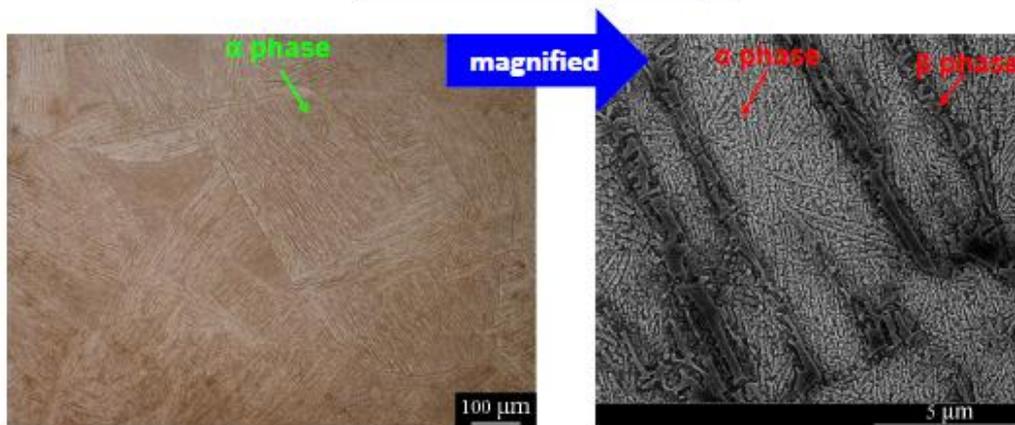
SEM

**Fig.8 Optical and SEM micrographs of Ti-6-4 alloy subjected to post-THP annealing treatment (704°C/2h/air cooling)**

the thicker α grains are obtained due to the effect of grain growth attributed by post-THP annealing treatment

17/31

AR+BST+THP+ANN(O<sub>2</sub>)



OM

SEM

**Fig.9 Optical and SEM micrographs of Ti-6-4 alloy subjected to post-THP annealing treatment with O<sub>2</sub>**

18/31

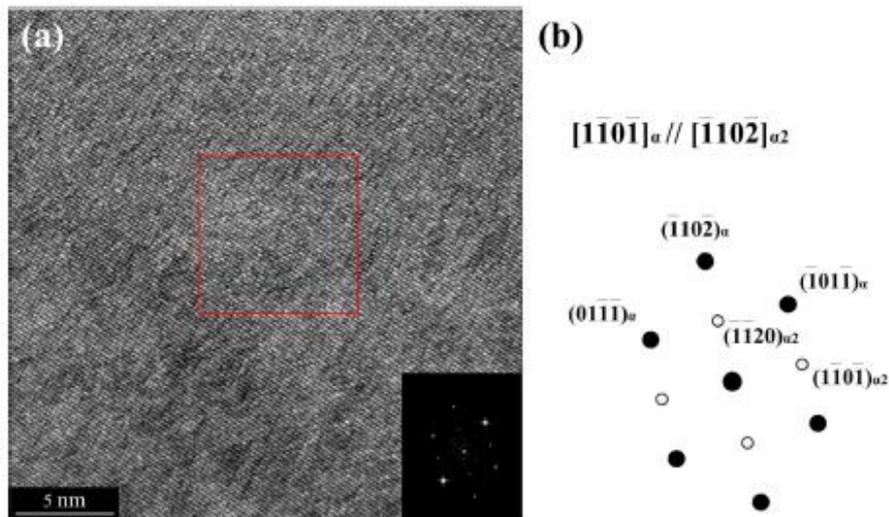
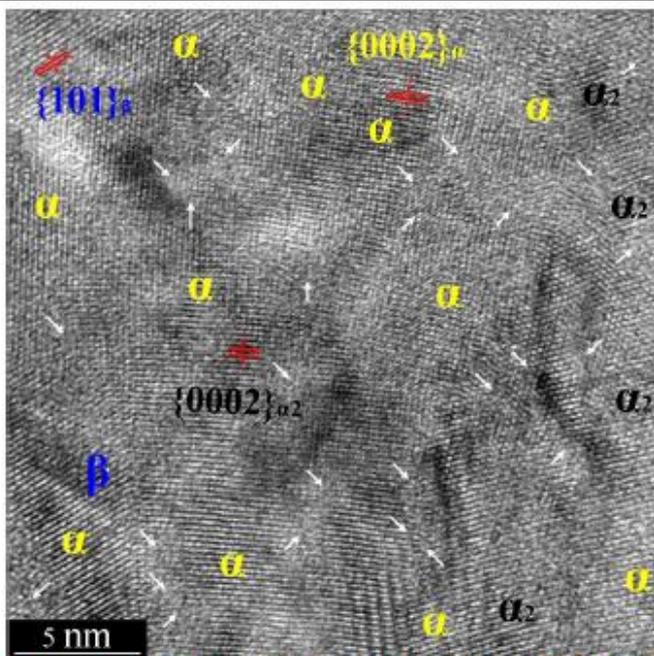


**Fig.10 (a) HRTEM micrograph of AR+BST+THP+ANN condition and its Fast Fourier Transform analysis of the framed area inserted (b) the corresponding schematic illustration of FFT pattern**

19/31



Relatively distorted region close to grain boundary are arrowed.

**Fig.11 HRTEM morphology of AR+BST+THP+ANN condition. The identified phases of  $\alpha$ ,  $\alpha_2$ , and  $\beta$  are marked, confirming the XRD result**

20/31

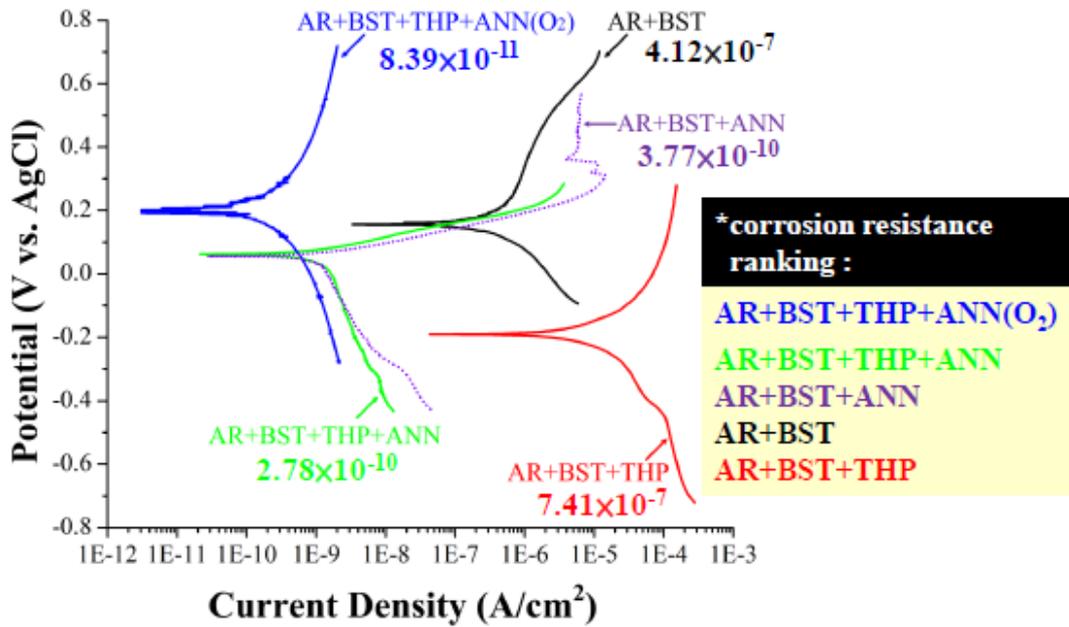


**Fig.12 Potential dynamic polarization curves of Ti-6-4 alloy after related treatments in 1N H<sub>2</sub>SO<sub>4</sub> solution (all measurements are carried out with produced oxide layer)**

21/31

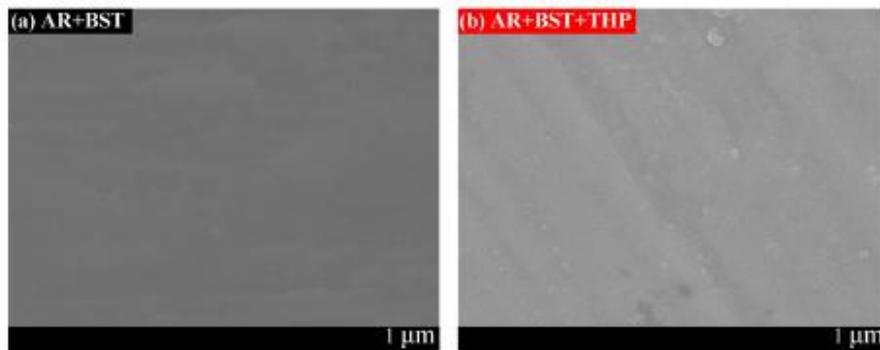


**Fig.13 SEM micrographs of the top surface of oxidized Ti-6-4 alloy of AR+BST and AR+BST+THP conditions**

**\*All the samples were ground with SiC abrasive papers and further polished with fine grade diamond paste before each stage treatment.**

22/31

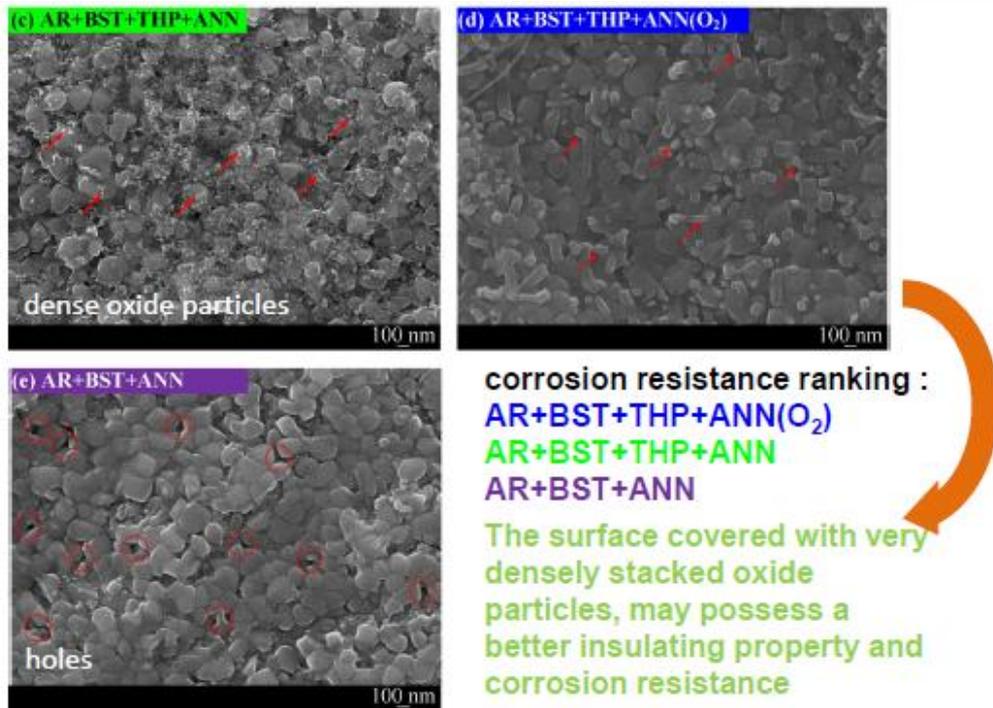


**Fig.13 SEM micrographs of the top surface of oxidized Ti-6-4 alloy after related treatments**

23/31

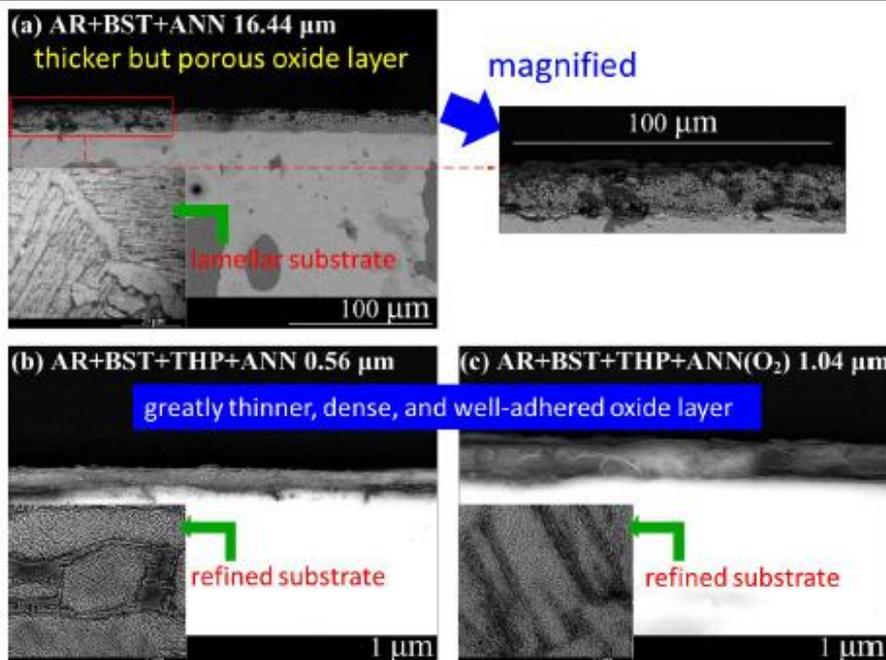


**Fig.14 Cross sectional SEM micrographs of oxidized Ti-6-4 alloy after related treatments**

**Refined Ti-6-4 substrate producing thinner oxide layer** 24/31

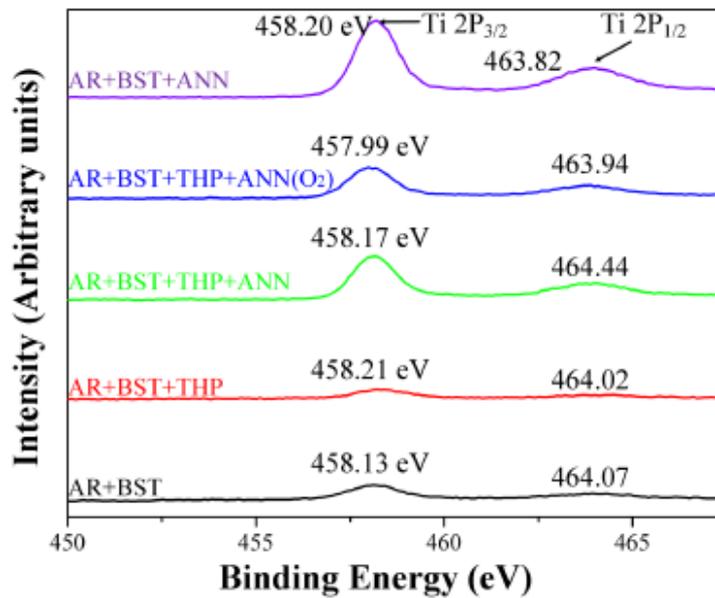


**Fig.16 XPS spectra of the Ti 2p region of the top surface after related treatments**

The Ti 2P<sub>3/2</sub> peak was positioned at about 458.2 eV, indicating oxidized Ti<sup>4+</sup> in the form of TiO<sub>2</sub> in agreement with the work of Wang et al. (JMR, Vol. 24, No. 12, pp3680-3688, 2009)

25/31

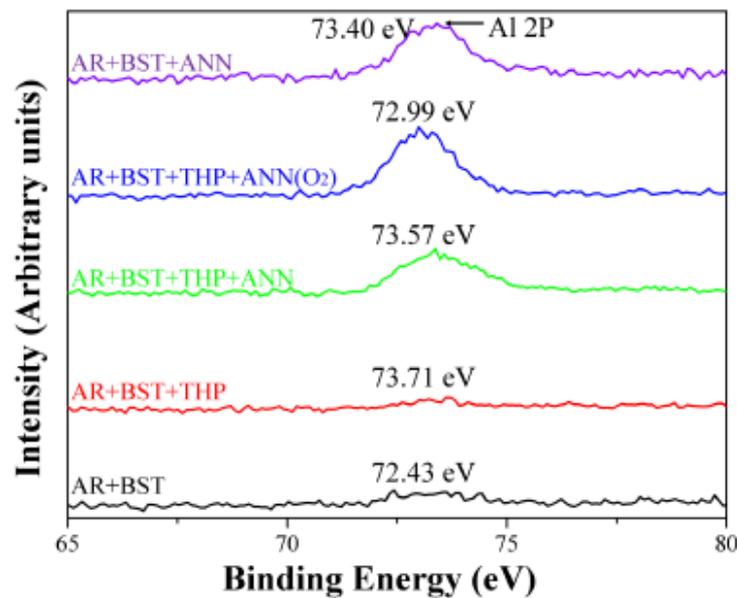


**Fig.17 XPS spectra of the V 2p region of the top surface after related treatments**

The Al 2P peak was positioned at about 73.2 eV, indicating oxidized Al<sup>3+</sup> in the form of Al<sub>2</sub>O<sub>3</sub> in agreement with the work of Wang et al. (JMR, Vol. 24, No. 12, pp3680-3688, 2009)

26/31

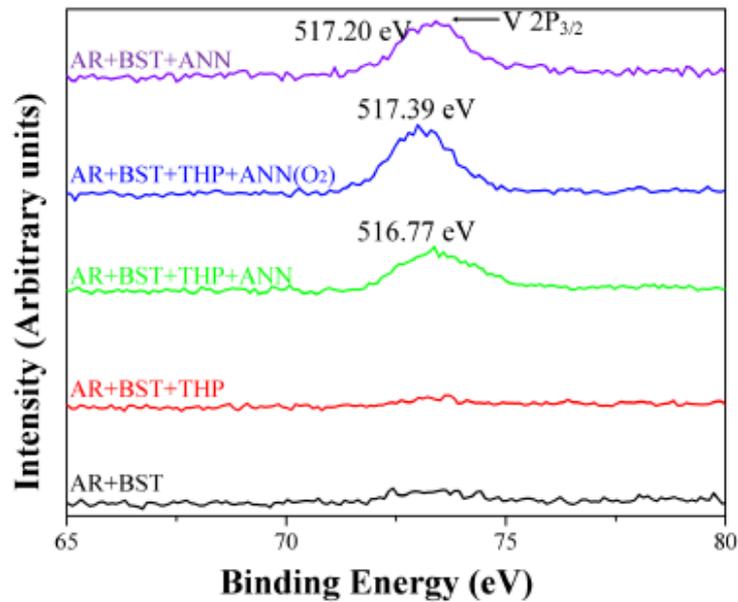


**Fig.18 XPS spectra of the V 2p region of the top surface after related treatments**

The V 2P peak was positioned at about 516.9 eV, indicating oxidized  $V^{5+}$  in the form of  $V_2O_5$  in agreement with the work of Wang et al. (JMR, Vol. 24, No.12, pp3680-3688,2009)

27/31

**TABLE II . Correlation between corrosion resistance and related of oxide layer.**

| Samples                         | Thickness ( $\mu\text{m}$ )<br>_Structure of<br>Oxide Layer | Composition of Oxide Layer<br>and Intensity of XPS<br>Ranking     |                                |                               | Corrosion<br>Resistance<br>Ranking         |
|---------------------------------|---|---|--------------------------------|-------------------------------|--|
|                                 |   | TiO <sub>2</sub>  | Al <sub>2</sub> O <sub>3</sub> | V <sub>2</sub> O <sub>5</sub> |  |
| AR+BST+THP+ANN(O <sub>2</sub> ) | 1.04_dense  | 3   | 1                              | 3                             | 1  |
| AR+BST+THP+ANN                  | 0.56_dense  | 2   | 2                              | 2                             | 2  |
| AR+BST+ANN                      | 16.44_porous  | 1   | 1                              | 1                             | 3  |
|                                 |   | *ranking 1 means obtained highest amount of related XPS intensity |                                |                               | *ranking 1 means best corrosion resistance |

\*the compactness of oxide layer is found a dominant factor affecting the corrosion resistance of Ti-6-4 alloy

\*Under the similar compactness of oxide layer, the Al<sub>2</sub>O<sub>3</sub> content becomes more crucial influencing the corrosion resistance of Ti-6-4 alloy

28/31

# Conclusions

- The thermohydrogen process results in the formation of refinement structures (refinement of  $\alpha$  matrix by breaking it into several pieces) and the precipitation of  $\alpha_2$  ( $\text{Ti}_3\text{Al}$ ) in Ti-6-4 alloy.



29/31

# Conclusions

- THP plus annealing treatment ( $704^\circ\text{C}$ ) together with controlled amount of oxygen (50cc/min) leads to the formation of thinner and denser oxide layers offering an effective process to improve the corrosion resistance of Ti-6-4 alloy.
- The  $\text{Al}_2\text{O}_3$  content becomes more crucial influencing the corrosion resistance of Ti-6-4 alloy under the similar structure of oxide layer.



30/31

**Thanks for  
your attention**

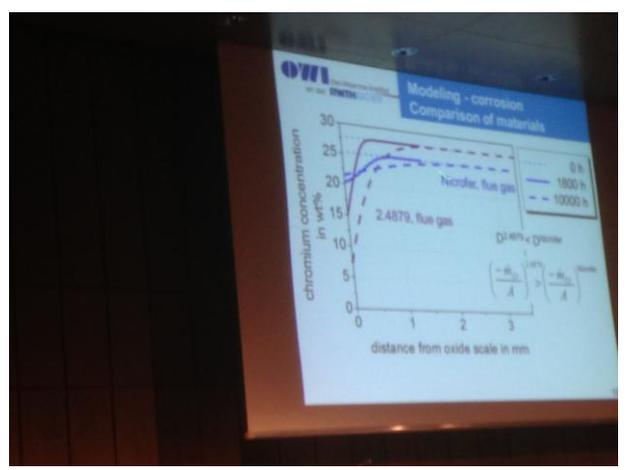
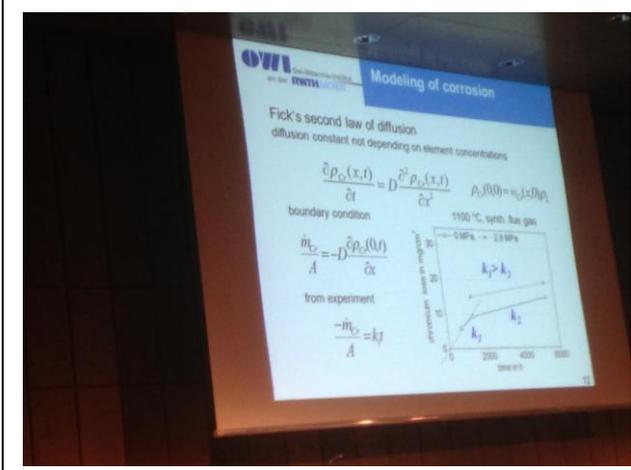
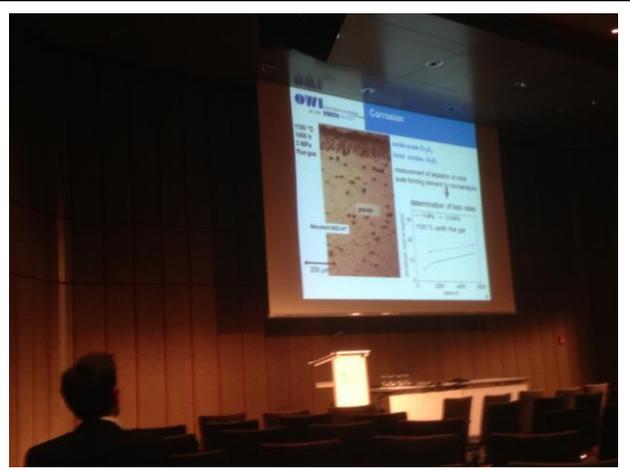


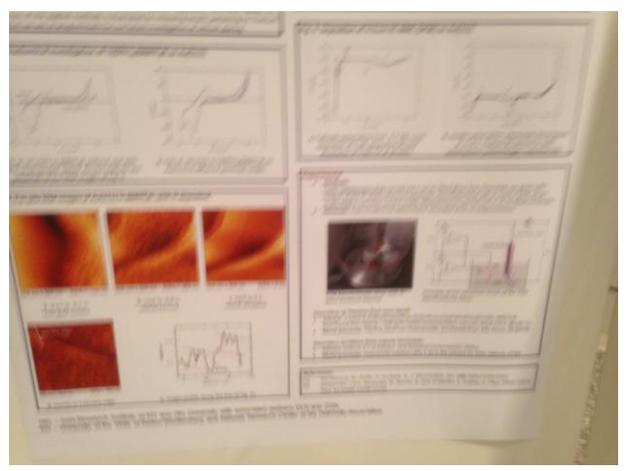
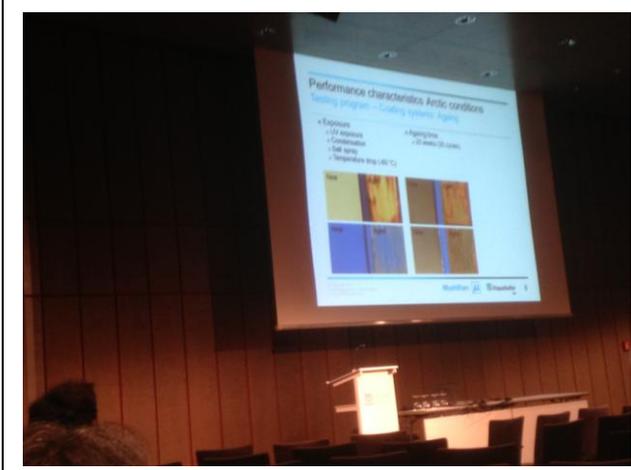
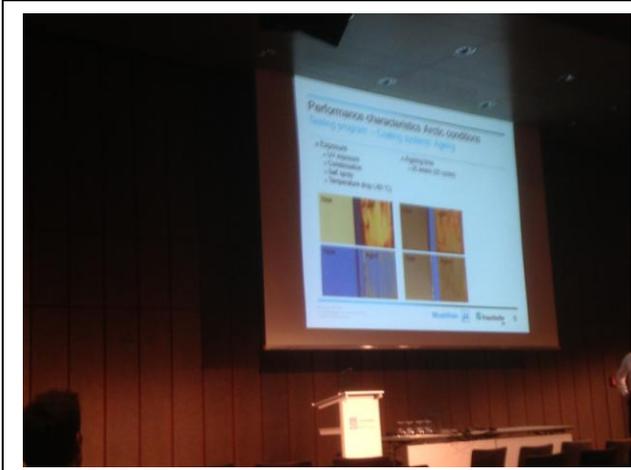
31/31

附件二：會中發表及參與研討之論文

本人參加德國 2013 「第二屆能源材料國際研討會」並受邀於會中發表論文及所指導論文海報所攝之照片







# 5月12日閱讀研討會論文海報之照片

### Role of reaction conditions for methane aromatization over various zeolites

Milan Bernauer<sup>1</sup>, Manon Guichard<sup>1</sup>, Rémy Sancier<sup>1</sup>, Vlastimil Fila<sup>1</sup>, Bohumil Bernauer<sup>1</sup>, Zdeněk Sobalík<sup>1</sup>  
<sup>1</sup> Heyrovský Institute of Physical Chemistry, Academy of Sciences of the Czech Republic, Czech Republic  
 Institute of Chemical Technology, Prague, Technická 5, 166 28 Prague 6, Czech Republic

**Introduction**  
 Methane dehydro-aromatization (MDA) is a non-oxidative process transforming methane to higher hydrocarbons (H). Due to equilibrium constraints the reaction must be realized at high temperatures (700 °C) and the main drawback is a fast deactivation of the catalyst by formation of coke deposits under reaction conditions. Several ways were investigated to overcome this problem, i.e. by addition of second metal component (Cu, Pt, Pd) or by addition of co-reactant (CO<sub>2</sub>, H<sub>2</sub>). The positive effect of increased pressure was identified by Hasekade group (2) in 2002 in laboratory experiments for NiCo/Al<sub>2</sub>O<sub>3</sub> and ZSM-5 zeolite catalysts. But this concept has not been widely considered, and is frequently missing in recent articles (see (3, 4)). Long term high pressure (up to 8 bar) experiments were carried out on zeolites (MCM-22, NiCo and ZSM-5) reported by (5). Experimental results show some similarities in trend of the position effect of increased pressure on the long term catalytic stability of the individual zeolite catalysts.

**Thermodynamic Study**  
 Effect of pressure on the chemical equilibrium of system containing H<sub>2</sub>, Ar, CH<sub>4</sub>, C<sub>2</sub>H<sub>4</sub>, C<sub>2</sub>H<sub>6</sub>, C<sub>3</sub>H<sub>6</sub>, C<sub>3</sub>H<sub>8</sub>, C<sub>4</sub>H<sub>6</sub>, C<sub>4</sub>H<sub>8</sub> system was investigated and calculated. The best way (10% of Ar and 80% of CH<sub>4</sub>) and temperature was 780 °C. Results are shown on following picture.

### Different types of cathode structures for lithium sulfur batteries

C. Scherr<sup>1</sup>, K.G. Schell<sup>1</sup>, E.C. Bucharsky<sup>1</sup>, S.Wagner<sup>1</sup>, J. Schneider<sup>2</sup> and M. J. Hoffmann<sup>1</sup>

**Working principle & problems**

- Incomplete usage of sulfur
- Drastic decrease of capacity during lifetime
- High self discharge rate
- High C-rate dependence

**Possible reasons**

- Formation of intermediate Li<sub>2</sub>S<sub>x</sub> species during discharge
- Disruption of Li<sub>2</sub>S<sub>x</sub> in liquid electrolyte
- Li<sub>2</sub>S<sub>x</sub> creating shuttle mechanism
- Formation of Li<sub>2</sub>S<sub>x</sub> with low reaction rate
- Formation of crystalline Li<sub>2</sub>S layers at the cathode and anode (Li<sup>+</sup> impermeable)

**Approach**

### Different types of cathode structures for lithium sulfur batteries

C. Scherr<sup>1</sup>, K.G. Schell<sup>1</sup>, E.C. Bucharsky<sup>1</sup>, S.Wagner<sup>1</sup>, J. Schneider<sup>2</sup> and M. J. Hoffmann<sup>1</sup>

**Working principle & problems**

- Incomplete usage of sulfur
- Drastic decrease of capacity during lifetime
- High self discharge rate
- High C-rate dependence

**Possible reasons**

- Formation of intermediate Li<sub>2</sub>S<sub>x</sub> species during discharge
- Disruption of Li<sub>2</sub>S<sub>x</sub> in liquid electrolyte
- Li<sub>2</sub>S<sub>x</sub> creating shuttle mechanism
- Formation of Li<sub>2</sub>S<sub>x</sub> with the reaction rate
- Formation of crystalline Li<sub>2</sub>S layers at the cathode and anode (Li<sup>+</sup> impermeable)

**Approach**

- Active material
- Carbon
- MBMI
- MBMI
- MBMI

**Results and Discussion**

Galvanostatic Experiments

### Study on the Safety Mechanism of Lithium-ion Battery by Hyperbranched Polymer Coated on Cathode

Chun-Chieh Lin<sup>a</sup>, Hung-Chun Wu<sup>b</sup>, Jing-Pin Pan<sup>a</sup>, and Nan-Lih Wu<sup>a</sup>  
<sup>a</sup>Department of Chemical Engineering, National Taiwan University, Taipei, Taiwan, R.O.C.  
<sup>b</sup>Material and Chemical Research Laboratories, Industrial Technology Research Institute, Hsinchu, Taiwan, R.O.C.

**Introduction & Objective**

The thermal runaway process of LIBs taking place under abuse conditions, such as over-charging and short circuit, has drawn much attention due to its detrimental to LIB applications. In spite of some countermeasures to develop, there is a consensus that the process is initiated by solid electrolyte interphase (SEI) breakdown, followed by interfacial electrolyte decomposition or reaction at the surface of charged active-materials, and finally by violent reaction of the cell components, such as anode electrolyte separator with the oxygen liberated from the cathode above certain critical temperature. The final step causes steep temperature escalation which could reach several hundred degrees within a few seconds in a practical abuse event. Another important factor that affects the initial heating process is peak-heating arising from short-circuit. Modified bismaleimide (MBMI) hyperbranched polymers as an additive material for LIBs-use electrolytes, has drawn much attention recently because it enhances the thermal stability and the cycle life of the battery. In this work, MBMI polymers is applied to Li(Ni<sub>0.8</sub>C<sub>0.2</sub>)Mn<sub>2</sub>O<sub>4</sub> cathode, and the same safety beneficial effect against thermal runaway is once again demonstrated. The object of this study is to investigate the underlying protecting mechanism enabled by the MBMI coating.

**Results and discussion**

**MBMI polymer**

Modified bismaleimide (MBMI) hyperbranched polymer

**Auto-heating Generation**

Nail penetration test (1-2 Ah)

The resistances of the charged electrode test

### Li(Ni<sub>0.8</sub>C<sub>0.2</sub>)Mn<sub>2</sub>O<sub>4</sub> cathode, and the same safety beneficial effect against thermal runaway mechanism enabled by the MBMI coating.

**Results and discussion**

**MBMI polymer**

Modified bismaleimide (MBMI) hyperbranched polymer

**The Chemical Heat Generation**

Electrochemical stability of MBMI coating

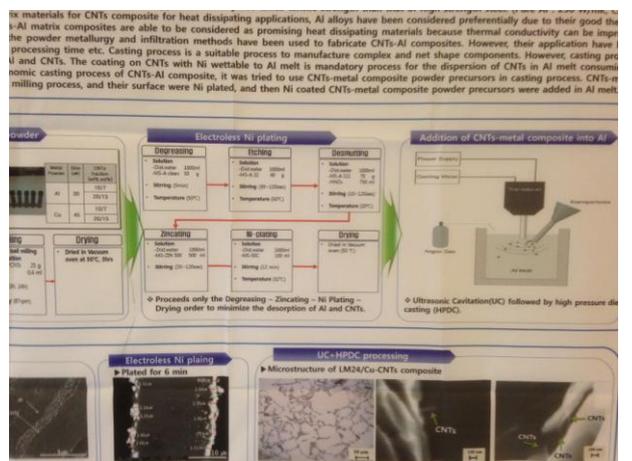
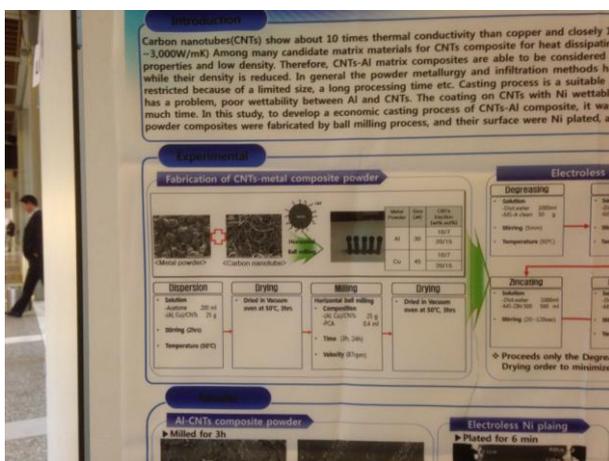
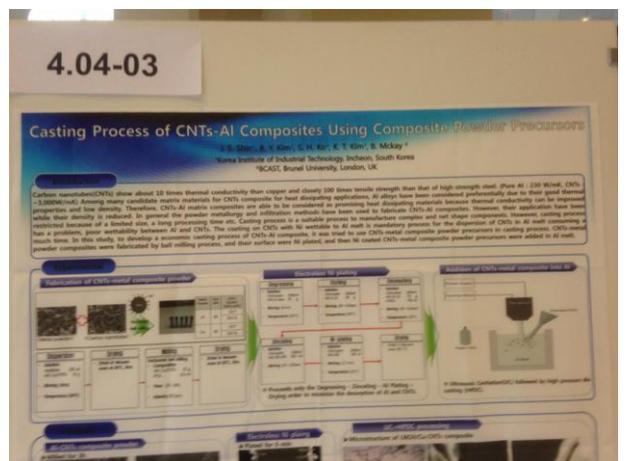
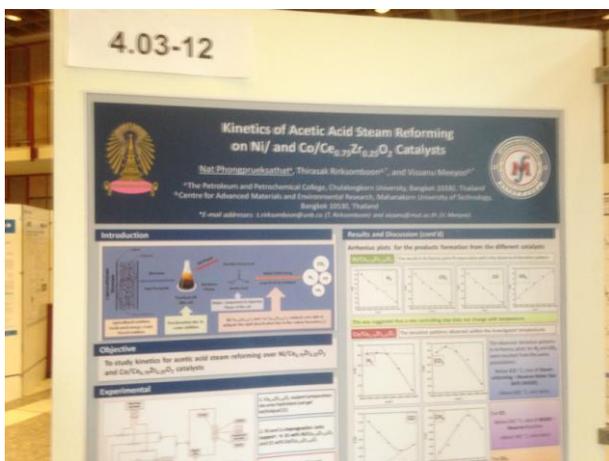
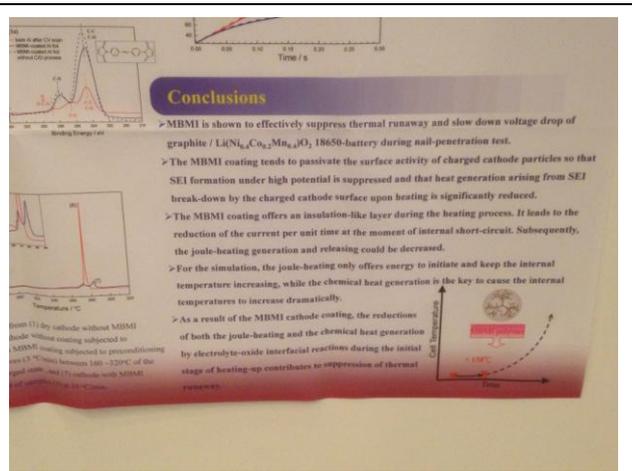
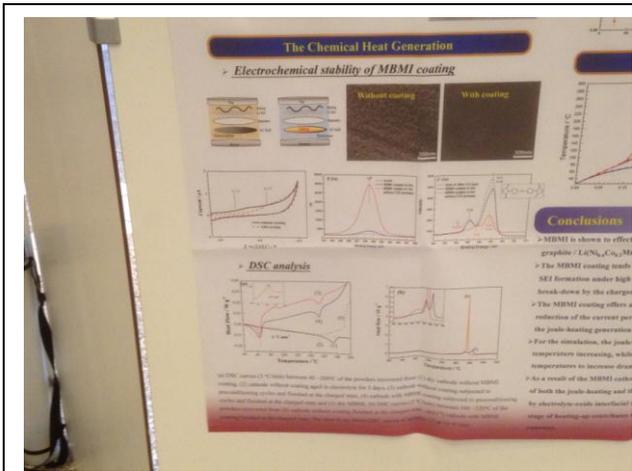
### Auto-heating Generation

Nail penetration test (1-2 Ah)

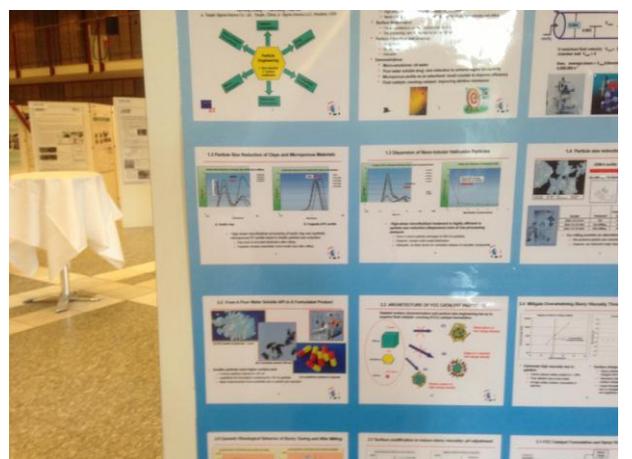
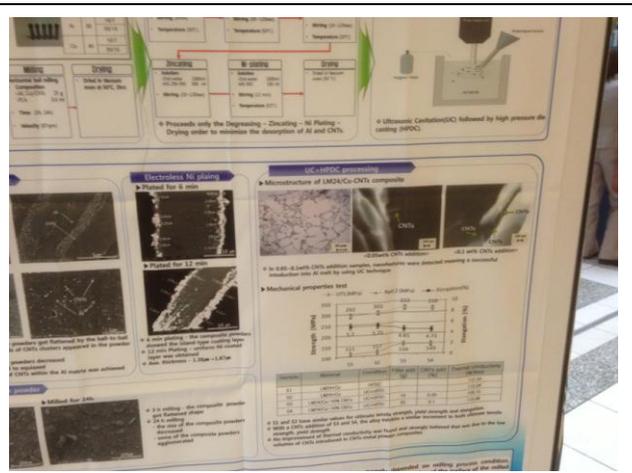
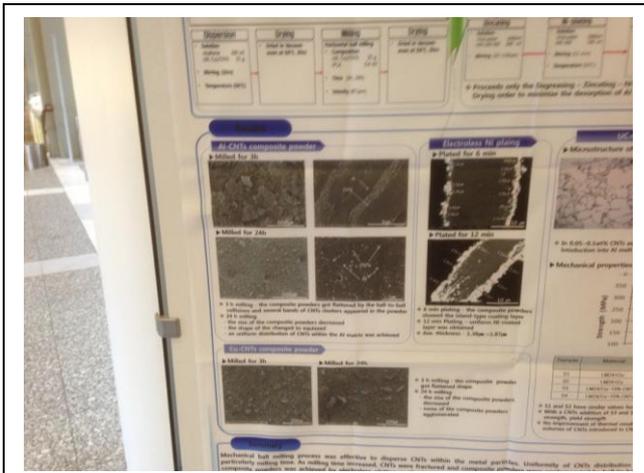
The resistances of the charged electrode test

**Simulation**

# 5月12日閱讀研討會論文海報之照片

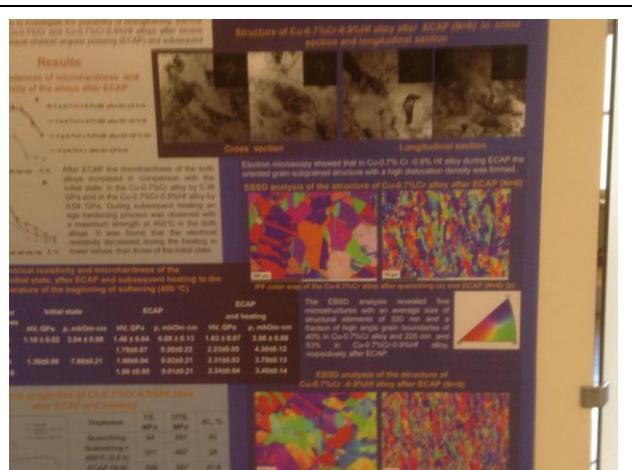
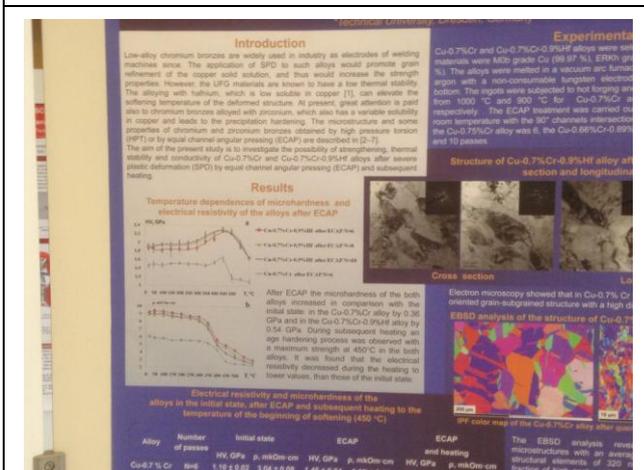
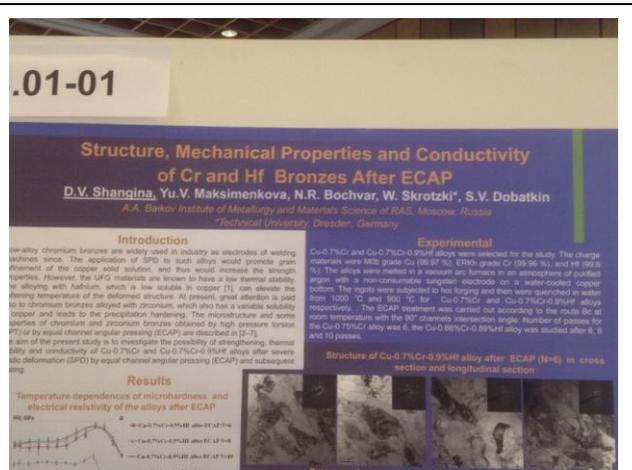
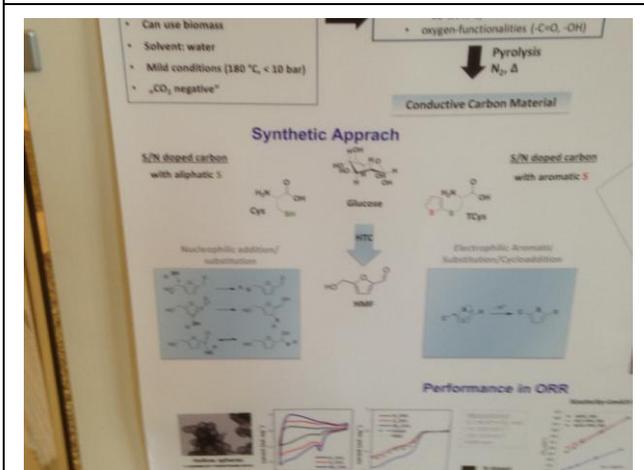
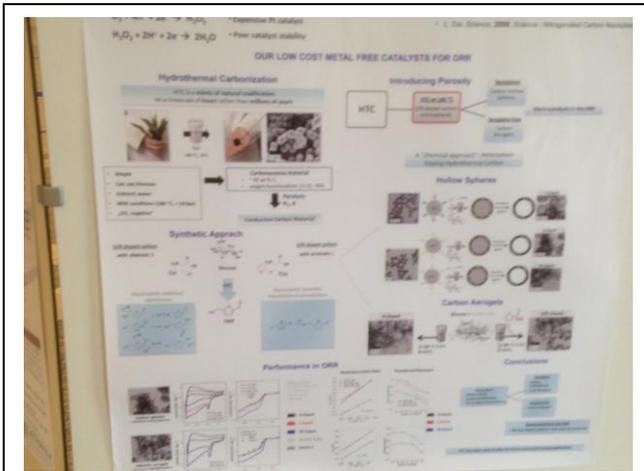


5月13日閱讀研討會論文海報之照片

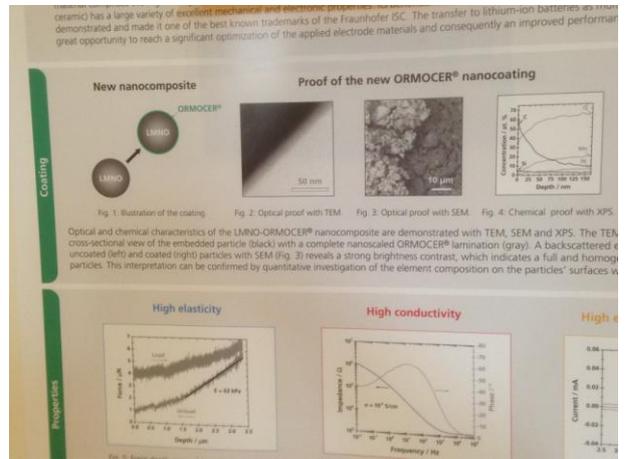
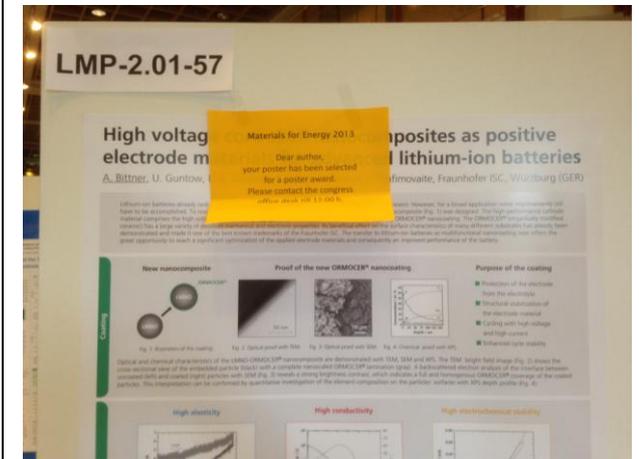
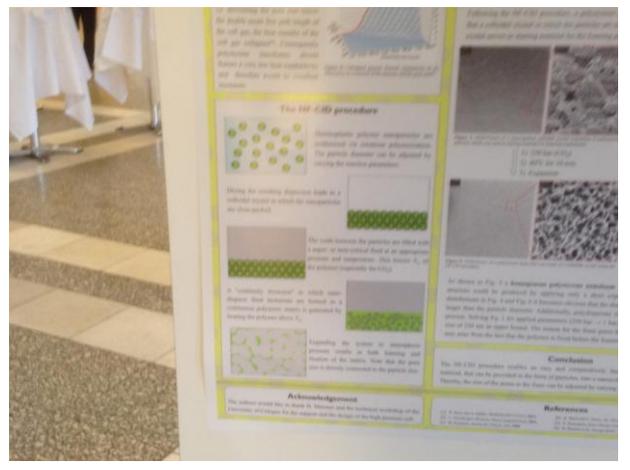
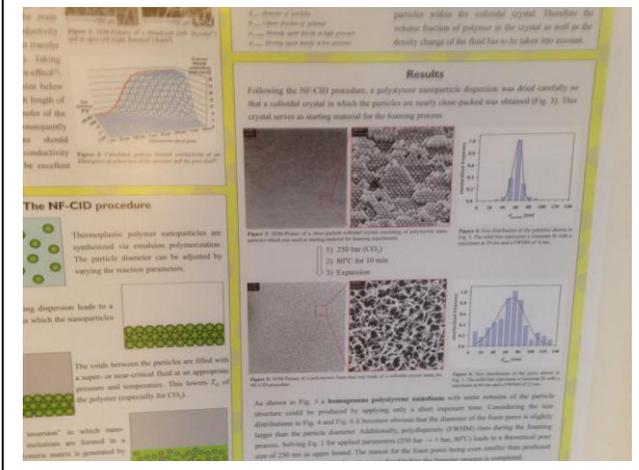
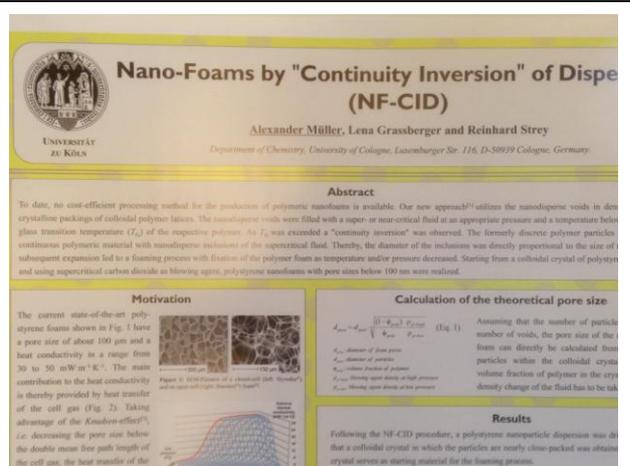
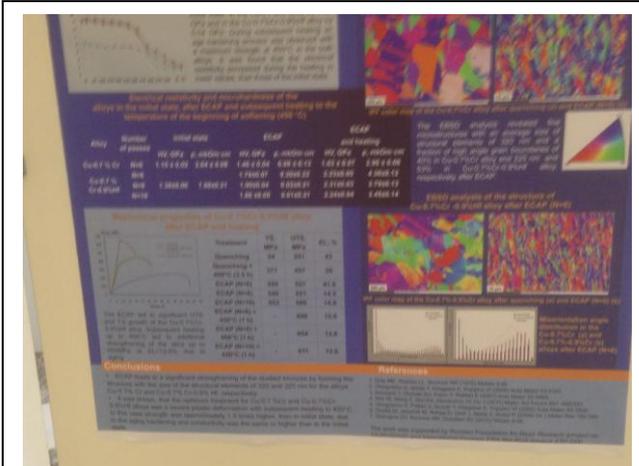




# 5月14日閱讀研討會論文海報之照片



5月14日閱讀研討會論文海報之照片



# 5月14日閱讀研討會論文海報之照片

TEM, SEM and XPS. The TEM bright field image (Fig. 2) shows the LMNO-ORMOCER® nanocomposite to a complete nanoscaled ORMOCER® lamination (gray). A backscattered electron analysis of the interface (Fig. 3) reveals a strong brightness contrast, which indicates a full and homogeneous ORMOCER® coverage of the LMNO particles. The quantitative investigation of the element composition on the particles' surfaces with XPS depth profile (Fig. 4).

Fig. 5: Force-depth curve of the ORMOCER® (gray) with fit of the elastic deformation (black). **High elasticity**

Fig. 6: Electrochemical impedance spectrum of the pure ORMOCER® containing LFP. **High conductivity**

Fig. 7: Cyclic voltammogram of the ORMOCER® containing LFP, with Li and Pt electrode. **High electrochemical stability**

The specific organic-inorganic network of the ORMOCER® leads to several remarkable properties. These properties include a modulus of elasticity of 63 kPa (Fig. 5), an ionic conductivity of  $10^{-2}$  S/cm (Fig. 6) and an electrochemical stability up to at least 5 V (Fig. 7). This makes the new coating the ideal refinement of high-performance battery materials, like the high voltage LMNO, and consequently enables a significant improvement in cycle stability and charge transfer kinetics of lithium-ion batteries.

**Improved cycling performance** **Improved charge transfer kinetics**

TEM, SEM and XPS. The TEM bright field image (Fig. 2) shows the LMNO-ORMOCER® nanocomposite to a complete nanoscaled ORMOCER® lamination (gray). A backscattered electron analysis of the interface (Fig. 3) reveals a strong brightness contrast, which indicates a full and homogeneous ORMOCER® coverage of the LMNO particles. The quantitative investigation of the element composition on the particles' surfaces with XPS depth profile (Fig. 4).

Fig. 5: Force-depth curve of the ORMOCER® (gray) with fit of the elastic deformation (black). **High elasticity**

Fig. 6: Electrochemical impedance spectrum of the pure ORMOCER® containing LFP. **High conductivity**

Fig. 7: Cyclic voltammogram of the ORMOCER® containing LFP, with Li and Pt electrode. **High electrochemical stability**

The specific organic-inorganic network of the ORMOCER® leads to several remarkable properties. These properties include a modulus of elasticity of 63 kPa (Fig. 5), an ionic conductivity of  $10^{-2}$  S/cm (Fig. 6) and an electrochemical stability up to at least 5 V (Fig. 7). This makes the new coating the ideal refinement of high-performance battery materials, like the high voltage LMNO, and consequently enables a significant improvement in cycle stability and charge transfer kinetics of lithium-ion batteries.

**Improved cycling performance** **Improved charge transfer kinetics**

The specific organic-inorganic network of the ORMOCER® leads to several remarkable properties. These properties include a modulus of elasticity of 63 kPa (Fig. 5), an ionic conductivity of  $10^{-2}$  S/cm (Fig. 6) and an electrochemical stability up to at least 5 V (Fig. 7). This makes the new coating the ideal refinement of high-performance battery materials, like the high voltage LMNO, and consequently enables a significant improvement in cycle stability and charge transfer kinetics of lithium-ion batteries.

Fig. 8: Cycling DC-CCCV against Li electrode with LFP in ECDEC as electrolyte. **Improved cycling performance**

Fig. 9: Corresponding charge curves at and discharge curves in 1C-CCCV. **Improved charge transfer kinetics**

LMNO-ORMOCER® nanocomposite electrodes were cycled up to 5 V vs. Li/Li⁺ with 1 C CC/CV by using the electrolyte LFP in ECDEC. The capacity retention of the electrode after 100 cycles (Fig. 8) and a significantly reduced polarization, which is indicated by the charge/discharge curves (Fig. 9).

**Conclusion:** A novel type of core-shell nanocomposite was achieved. Its specific ORMOCER® nanocoating provides various excellent properties, like a high elasticity, a high ionic conductivity and a remarkable electrochemical stability. It was demonstrated that the coating of LMNO with ORMOCER® leads to a significantly improved electrochemical performance. This improvement is expressed in a more than 15% better capacity retention of the electrode after 100 cycles (Fig. 8) and a significantly reduced polarization, which is indicated by the charge/discharge curves (Fig. 9).

This research is supported by the financial support of the BMBWF and the Alexander Humboldt Foundation. We gratefully acknowledge the technical assistance of the BMBWF and the Alexander Humboldt Foundation. We gratefully acknowledge the technical assistance of the BMBWF and the Alexander Humboldt Foundation.

The specific organic-inorganic network of the ORMOCER® leads to several remarkable properties. These properties include a modulus of elasticity of 63 kPa (Fig. 5), an ionic conductivity of  $10^{-2}$  S/cm (Fig. 6) and an electrochemical stability up to at least 5 V (Fig. 7). This makes the new coating the ideal refinement of high-performance battery materials, like the high voltage LMNO, and consequently enables a significant improvement in cycle stability and charge transfer kinetics of lithium-ion batteries.

Fig. 8: Cycling DC-CCCV against Li electrode with LFP in ECDEC as electrolyte. **Improved cycling performance**

Fig. 9: Corresponding charge curves at and discharge curves in 1C-CCCV. **Improved charge transfer kinetics**

LMNO-ORMOCER® nanocomposite electrodes were cycled up to 5 V vs. Li/Li⁺ with 1 C CC/CV by using the electrolyte LFP in ECDEC. The capacity retention of the electrode after 100 cycles (Fig. 8) and a significantly reduced polarization, which is indicated by the charge/discharge curves (Fig. 9).

**Conclusion:** A novel type of core-shell nanocomposite was achieved. Its specific ORMOCER® nanocoating provides various excellent properties, like a high elasticity, a high ionic conductivity and a remarkable electrochemical stability. It was demonstrated that the coating of LMNO with ORMOCER® leads to a significantly improved electrochemical performance. This improvement is expressed in a more than 15% better capacity retention of the electrode after 100 cycles (Fig. 8) and a significantly reduced polarization, which is indicated by the charge/discharge curves (Fig. 9).

This research is supported by the financial support of the BMBWF and the Alexander Humboldt Foundation. We gratefully acknowledge the technical assistance of the BMBWF and the Alexander Humboldt Foundation.

WASILIOS SIOZIOS\*, Tobias Placke, Andreas Heckmann, Stefano Passerini, Martin Winter  
University of Münster, Institute of Physical Chemistry, MEET Battery Research Center, Corneusstraße 46, 48149 Münster, Germany

## Surface modification of carbons by elevated temperature gas treatments for an improved solid electrolyte interphase formation

**Introduction**  
Currently, graphitic carbons are the most commonly used anode materials. Since lithium-ion cells typically operate beyond the electrochemical stability window of the organic electrolytes, electrolyte decomposition occurs. Decomposition products form a protective film at the anode which, in an ideal case, acts as an electronically insulating layer, stopping further electrolyte decomposition, while still permitting the transport of lithium ions. This solid electrolyte interphase (SEI) is associated with irreversible consumption of lithium and electrolyte. [1,2]

**Relevance of graphite surface properties**  
Surface properties of graphite influence the formation of the SEI layer.  
Transport of lithium ions during charge-discharge cycling processes occurs via the prismatic surfaces.  
Chemical composition of the prismatic surfaces has significant impact on the electrochemical performance.  
Ratio of the basal plane surface area to the "non-basal plane surface" area is an important factor in determining the dependence of irreversible charge losses to the specific surface area [3].

**Methods**  
Graphite surface modifications (SLP30 & T44 graphite by TIMCAL®) were performed by an elevated temperature treatment with oxygen (temperature range: 300°C to 600°C).

## treatments for an improved solid electrolyte interphase formation

**Introduction**  
Currently, graphitic carbons are the most commonly used anode materials. Since lithium-ion cells typically operate beyond the electrochemical stability window of the organic electrolytes, electrolyte decomposition occurs. Decomposition products form a protective film at the anode which, in an ideal case, acts as an electronically insulating layer, stopping further electrolyte decomposition, while still permitting the transport of lithium ions. This solid electrolyte interphase (SEI) is associated with irreversible consumption of lithium and electrolyte. [1,2]

**Relevance of graphite surface properties**  
Surface properties of graphite influence the formation of the SEI layer.  
Transport of lithium ions during charge-discharge cycling processes occurs via the prismatic surfaces.  
Chemical composition of the prismatic surfaces has significant impact on the electrochemical performance.  
Ratio of the basal plane surface area to the "non-basal plane surface" area is an important factor in determining the dependence of irreversible charge losses to the specific surface area [3].

**Methods**  
Graphite surface modifications (SLP30 & T44 graphite by TIMCAL®) were performed by an elevated temperature treatment with oxygen (temperature range: 300°C to 600°C).

# 5月14日閱讀研討會論文海報之照片

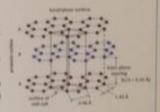
## Surface treatments for an improved solid electrolyte interphase

### Introduction

Currently, graphitic carbons are the most commonly used anode materials. Since lithium-ion cells typically operate beyond the electrochemical stability window of the organic electrolytes, electrolyte decomposition occurs. Decomposition products form a protective film at the anode which, in an ideal case, acts as an electronically insulating layer, stopping further electrolyte decomposition, while still permitting the transport of lithium ions. This solid electrolyte interphase (SEI) is associated with irreversible consumption of lithium and electrolyte. [1,2]

### Relevance of graphite surface properties

- Surface properties of graphite influence the formation of the SEI layer
- Transport of lithium ions during charge-discharge cycling processes occurs via the prismatic surfaces
- Chemical composition of the prismatic surfaces has significant impact on the electrochemical performance
- Ratio of the basal plane surface area to the "non-basal plane surface" area is an important factor in determining the dependence of irreversible charge losses to the specific surface area [3]



### Methods

- Graphite surface modifications (SLP30 & T44 graphite by TIMCAL<sup>®</sup>) were performed by an elevated temperature treatment with oxygen (temperature range: 480°C to 620°C).

### Methods

- Graphite surface modifications (SLP30 & T44 graphite by TIMCAL<sup>®</sup>) were performed by an elevated temperature treatment with oxygen (temperature range: 480°C to 600°C), CO<sub>2</sub> (temperature range: 700°C to 1000°C) and NH<sub>3</sub> at 1000°C
- Graphite modifications were performed in a quartz glass tube within a tube furnace
- Nitrogen adsorption measurements were performed using an ASAP 2020 apparatus (Micromeritics). DFT Plus<sup>®</sup> software was used to calculate the adsorptive potential distributions
- Thermogravimetric analysis was performed on a TGA Q5000 at HiRes<sup>®</sup> system (TA instruments) to determine and to identify the graphite surface groups [4]
- Electrode topos: 95 wt.% of active material (either pristine or heat-treated graphite) and 5 wt.% PVDF/Kynar<sup>®</sup> 761.
- Electrochemical investigations in Swagelok<sup>®</sup>-type 1-cells; Electrolyte: EC/DEC 3:7 wt.% with 1 M LiPF<sub>6</sub>; Constant current 0.5C; charge/discharge rate with cut-off potential of 20 mV vs. Li/Li<sup>+</sup> for charge and 1500 mV vs. Li/Li<sup>+</sup> for discharge

### SEM images of pristine and modified graphites



### Identify the graphite surface groups [4]

- Electrode topos: 95 wt.% of active material (either pristine or heat-treated graphite) and 5 wt.% PVDF/Kynar<sup>®</sup> 761.
- Electrochemical investigations in Swagelok<sup>®</sup>-type 1-cells; Electrolyte: EC/DEC 3:7 wt.% with 1 M LiPF<sub>6</sub>; Constant current 0.5C; charge/discharge rate with cut-off potential of 20 mV vs. Li/Li<sup>+</sup> for charge and 1500 mV vs. Li/Li<sup>+</sup> for discharge

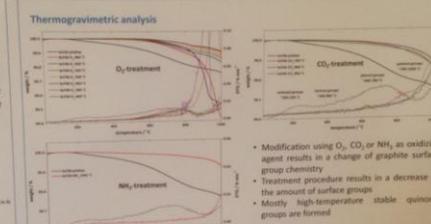
### SEM images of pristine and modified graphites



www.uni-muenster.de/MEET

## Improved solid electrolyte interphase formation

### Thermogravimetric analysis

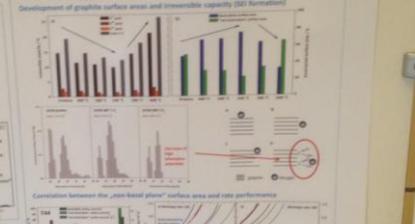


- Modification using O<sub>2</sub>, CO<sub>2</sub> or NH<sub>3</sub> as oxidizing agent results in a change of graphite surface group chemistry
- Treatment procedure results in a decrease of the amount of surface groups
- Mostly high-temperature stable quinone groups are formed

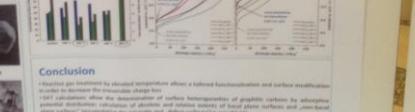
### Development of graphite surface areas and irreversible capacity (SEI formation)



### Development of graphite surface areas and irreversible capacity (SEI formation)



### Correlation between the "non-basal plane" surface area and rate performance



### Conclusion

Surface gas treatment by elevated temperature allows a tailored functionalization and surface modification in order to decrease the irreversible charge loss

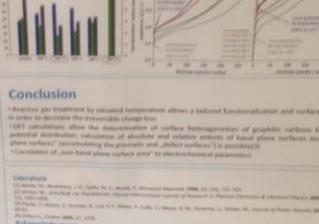
SEI calculations allow the determination of surface heterogeneities of graphite carbons by adsorptive potential distribution, calculation of absolute and relative contents of basal plane surface and "non-basal plane surface" (heterogeneity can provide the surface heterogeneity) is possible

Correlation of "non-basal plane surface area" to electrochemical performance

### SEM images of pristine and modified graphites



### Correlation between the "non-basal plane" surface area and rate performance



### Conclusion

Surface gas treatment by elevated temperature allows a tailored functionalization and surface modification in order to decrease the irreversible charge loss

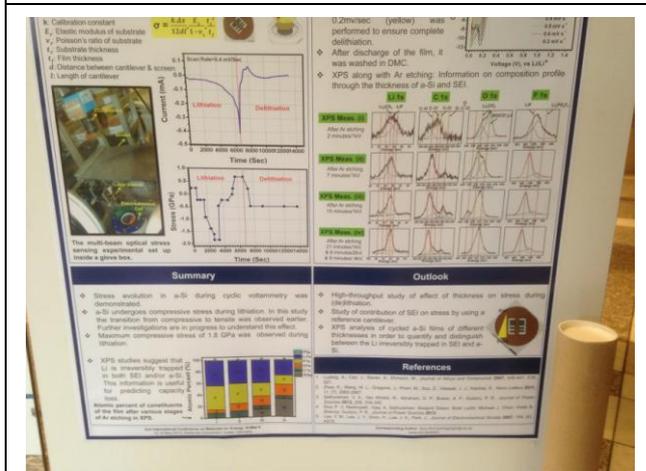
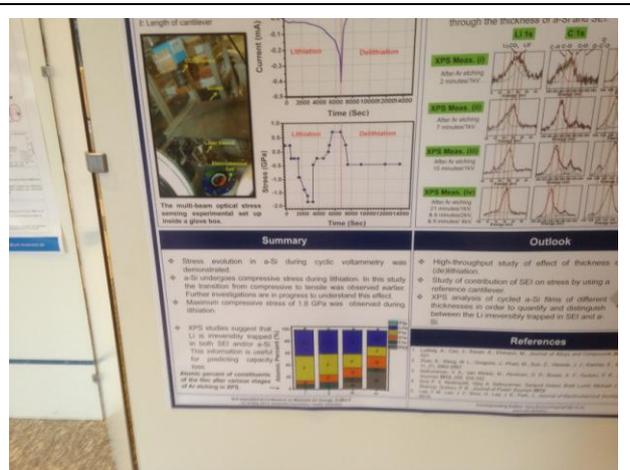
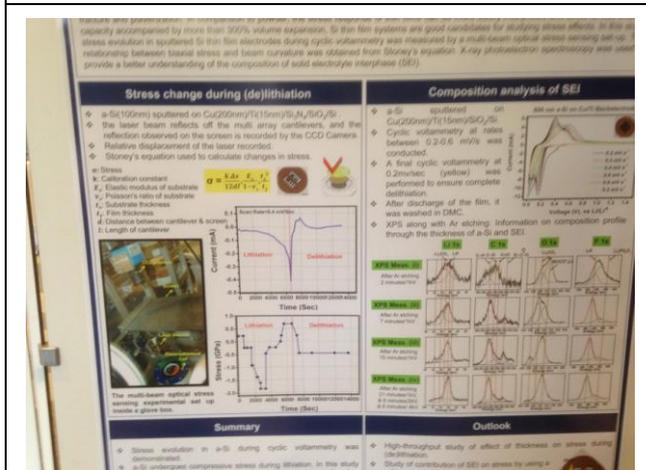
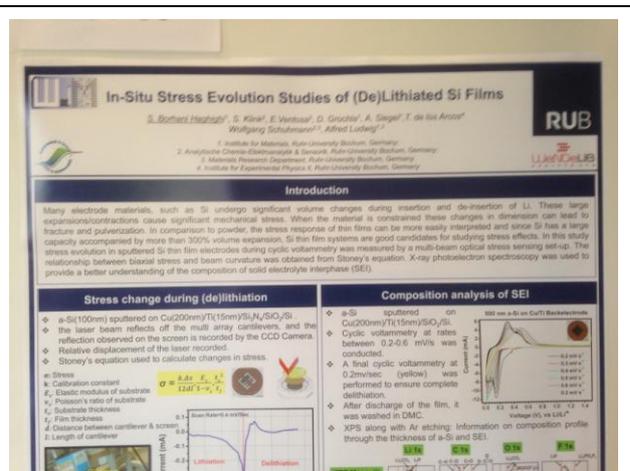
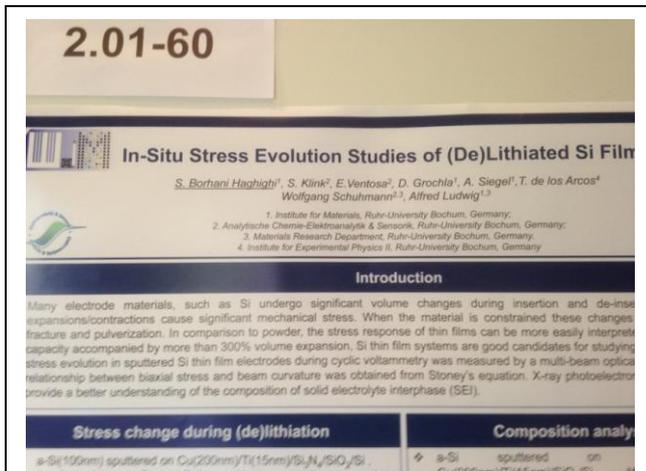
SEI calculations allow the determination of surface heterogeneities of graphite carbons by adsorptive potential distribution, calculation of absolute and relative contents of basal plane surface and "non-basal plane surface" (heterogeneity can provide the surface heterogeneity) is possible

Correlation of "non-basal plane surface area" to electrochemical performance

www.uni-muenster.de/MEET

\* v.slozios@uni-muenster.de

5月15日閱讀研討會論文海報之照片



5月15日閱讀研討會論文海報之照片

**In situ and ex situ studies of lithium nucleation and dendritic growth during electroplating**  
 Jens Stieger<sup>1</sup>, Dominik Kramer<sup>1</sup>, Steven T. Boles<sup>1</sup>, Reiner Mönig<sup>1</sup>  
<sup>1</sup> Helmholtz Institute Ulm for Electrochemical Energy Storage (HIU), Ulm, Germany

**Motivation and Aim**

- Lithium plating can happen in all lithium ion batteries for high charging rates, especially at low T
- Dendrites or needle-like growth can cause safety problems
- SEM images of electroplated Li showing needle-like lithium
- Controlled plating could be achieved
- Whisker removal agents could be used
- Understanding dendritic growth (DGG) is key

**Experimental**

- Microarray SEM Electrode holder with electroplating transfer system
- Microarray holder for optical microscopy
- Microarray substrate (measured by laser diffraction [1])

**In situ Stress measurements**

- Current, potential and stress during a CV
- Temperature variations of the stress are measured
- Measurement of stress in surface layers

**Growth of lithium whiskers in vacuum**

- Lithium is deposited in situ in a vacuum with heating filtration
- SEM images of Li whiskers growing on substrate
- Temperature variations of the stress are measured
- Measurement of stress in surface layers

**Growth modes**

- Cu-cooper substrates: stress lithium whiskers are dependent on copper
- The fast and dense growth of whiskers is observed in copper
- SEM image of Li deposit

**Insertion mechanism**

- Lithium insertion is proven between opening gaps of the copper

**SEM images of Li whiskers growing on a substrate at room temperature**

**Experimental**

- Microarray SEM Electrode holder with electroplating transfer system
- Microarray holder for optical microscopy
- Microarray substrate (measured by laser diffraction [1])

**In situ Stress measurements**

- Current, potential and stress during a CV
- Temperature variations of the stress are measured
- Measurement of stress in surface layers

**Growth modes**

- Cu-cooper substrates: stress lithium whiskers are dependent on copper
- The fast and dense growth of whiskers is observed in copper
- SEM image of Li deposit

**Insertion mechanism**

- Lithium insertion is proven between opening gaps of the copper

**Summary**

- We highlight that Li whiskers and dendrites are dependent on insertion mechanism
- Analysis of the SEM and of the stress
- Analysis of the stress in the surface

**2.01-42**

**XRD total scattering and pair distribution function (PDF) measurements on  $\text{LiNi}_{0.5}\text{Mn}_{1.5}\text{O}_4$  spinel**  
 M. Yavuz<sup>1,2</sup>, N. K. Yavuz<sup>2</sup>, M. Knapp<sup>1,2</sup>, K. Nikolowski<sup>1,2</sup>, H. Ehrenberg<sup>1,2</sup>  
<sup>1</sup>Helmholtz Institute Ulm (HIU) Electrochemical Energy Storage,  
<sup>2</sup>Institute for Applied Materials-Energy Storage Systems (IAM-ESS), Karlsruhe Institute of Technology (KIT), Herman-von-Helmholtz Platz 1, 76344 Eggenstein-Leopoldshafen, Germany

**Introduction**

The knowledge about the local arrangement of the atoms in Li-ion battery materials is of central importance since it is correlated to parameters like capacity, rate capability, reversibility and life time. For this purpose the Pair Distribution Function (PDF)/Total scattering method is used to obtain information about the structural arrangement and about the disorder or local ordering that occurs due to (de)intercalation of lithium, which is correlated to degradation and fatigue in Li-ion battery materials. The PDF analysis/Total scattering technique, gives information about the local atomic arrangement in materials as well as the long range (average) structure. It mainly gives the probability of finding any two atoms at given distance "r" and it can be considered as a bond length distribution.

The spinel  $\text{LiNi}_{0.5}\text{Mn}_{1.5}\text{O}_4$  cathode shows impressive electrochemical performance like large reversible capacity at high operating voltage around 4.7 V which makes it a promising and suitable cathode material for high energy battery applications [1]. In this material all the Mn is expected to be in  $\text{Mn}^{4+}$  form, not  $\text{Mn}^{3+}$ , which is well-known as Jahn-Teller ion causing structural instability. But usually small amounts of  $\text{Mn}^{3+}$  remains as a result of oxygen deficiency after the high temperature synthesis process [2]. In this study the  $\text{LiNi}_{0.5}\text{Mn}_{1.5}\text{O}_4$  samples were synthesized by a citric acid-assisted sol-gel method using metal acetates as precursors at different re-annealing temperatures. The effect of temperature on the structure of the material has been studied with pair distribution function (PDF) analysis.

**Experimental Details**

X-ray diffraction experiments were carried out at the High Resolution Powder Diffraction beamline (P02-1) at PETRA-III, DESY, using X-rays with an energy of 60 keV ( $\lambda=0.20726 \text{ \AA}$ ). The 2D diffraction patterns of  $\text{LiNi}_{0.5}\text{Mn}_{1.5}\text{O}_4$  samples in kapton capillary ( $\varnothing 0.4037 \text{ mm}$ ) are recorded on the flat panel detector (Perkin Elmer) in 2 min, and the sample-detector distance was approximately 400mm. The max. G-value was about  $24 \text{ \AA}^{-1}$ .

**Results**

The X-ray diffraction patterns of  $\text{LiNi}_{0.5}\text{Mn}_{1.5}\text{O}_4$  cathode shows impressive electrochemical performance like large reversible capacity at high operating voltage around 4.7 V which makes it a promising and suitable cathode material for high energy battery applications [1]. In this material all the Mn is expected to be in  $\text{Mn}^{4+}$  form, not  $\text{Mn}^{3+}$ , which is well-known as Jahn-Teller ion causing structural instability. But usually small amounts of  $\text{Mn}^{3+}$  remains as a result of oxygen deficiency after the high temperature synthesis process [2]. In this study the  $\text{LiNi}_{0.5}\text{Mn}_{1.5}\text{O}_4$  samples were synthesized by a citric acid-assisted sol-gel method using metal acetates as precursors at different re-annealing temperatures. The effect of temperature on the structure of the material has been studied with pair distribution function (PDF) analysis.

The program PDFgetX2 was used to convert 2-D images to 1-D diffraction patterns using circle integration. The sample-detector distance, beam center position and tilt angle of the detector were calibrated using LaB<sub>6</sub>.

Using the PDFgetX2 program, standard data corrections were implemented including subtraction of background scattering, sample absorption, multiple scattering, X-ray polarization, unstrained Lorentz intensity and then the PDFs were obtained. The obtained experimental pair distribution functions  $G(r)$  were refined and modeled in real space using PDFgui software. During the PDF refinement, the standard parameter values ( $D_{\text{min}}$  and  $D_{\text{max}}$ ) were used that were determined from the refinement of the standard material LaB<sub>6</sub> in PDFgui software.

**HIU) Electrochemical Energy Storage, Energy Storage Systems (IAM-ESS), Karlsruhe Institute of Technology (KIT), Herman-von-Helmholtz Platz 1, Eggenstein-Leopoldshafen, Germany**

**Introduction**

The knowledge about the local arrangement of the atoms in Li-ion battery materials is of central importance since it is correlated to parameters like capacity, rate capability, reversibility and life time. For this purpose the Pair Distribution Function (PDF)/Total scattering method is used to obtain information about the structural arrangement and about the disorder or local ordering that occurs due to (de)intercalation of lithium, which is correlated to degradation and fatigue in Li-ion battery materials. The PDF analysis/Total scattering technique, gives information about the local atomic arrangement in materials as well as the long range (average) structure. It mainly gives the probability of finding any two atoms at given distance "r" and it can be considered as a bond length distribution.

The spinel  $\text{LiNi}_{0.5}\text{Mn}_{1.5}\text{O}_4$  cathode shows impressive electrochemical performance like large reversible capacity at high operating voltage around 4.7 V which makes it a promising and suitable cathode material for high energy battery applications [1]. In this material all the Mn is expected to be in  $\text{Mn}^{4+}$  form, not  $\text{Mn}^{3+}$ , which is well-known as Jahn-Teller ion causing structural instability. But usually small amounts of  $\text{Mn}^{3+}$  remains as a result of oxygen deficiency after the high temperature synthesis process [2]. In this study the  $\text{LiNi}_{0.5}\text{Mn}_{1.5}\text{O}_4$  samples were synthesized by a citric acid-assisted sol-gel method using metal acetates as precursors at different re-annealing temperatures. The effect of temperature on the structure of the material has been studied with pair distribution function (PDF) analysis.

**Experimental Details**

X-ray diffraction experiments were carried out at the High Resolution Powder Diffraction beamline (P02-1) at PETRA-III, DESY, using X-rays with an energy of 60 keV ( $\lambda=0.20726 \text{ \AA}$ ). The 2D diffraction patterns of  $\text{LiNi}_{0.5}\text{Mn}_{1.5}\text{O}_4$  samples in kapton capillary ( $\varnothing 0.4037 \text{ mm}$ ) are recorded on the flat panel detector (Perkin Elmer) in 2 min, and the sample-detector distance was approximately 400mm. The max. G-value was about  $24 \text{ \AA}^{-1}$ .

**Results**

The X-ray diffraction patterns of  $\text{LiNi}_{0.5}\text{Mn}_{1.5}\text{O}_4$  cathode shows impressive electrochemical performance like large reversible capacity at high operating voltage around 4.7 V which makes it a promising and suitable cathode material for high energy battery applications [1]. In this material all the Mn is expected to be in  $\text{Mn}^{4+}$  form, not  $\text{Mn}^{3+}$ , which is well-known as Jahn-Teller ion causing structural instability. But usually small amounts of  $\text{Mn}^{3+}$  remains as a result of oxygen deficiency after the high temperature synthesis process [2]. In this study the  $\text{LiNi}_{0.5}\text{Mn}_{1.5}\text{O}_4$  samples were synthesized by a citric acid-assisted sol-gel method using metal acetates as precursors at different re-annealing temperatures. The effect of temperature on the structure of the material has been studied with pair distribution function (PDF) analysis.

The program PDFgetX2 was used to convert 2-D images to 1-D diffraction patterns using circle integration. The sample-detector distance, beam center position and tilt angle of the detector were calibrated using LaB<sub>6</sub>.

Using the PDFgetX2 program, standard data corrections were implemented including subtraction of background scattering, sample absorption, multiple scattering, X-ray polarization, unstrained Lorentz intensity and then the PDFs were obtained. The obtained experimental pair distribution functions  $G(r)$  were refined and modeled in real space using PDFgui software. During the PDF refinement, the standard parameter values ( $D_{\text{min}}$  and  $D_{\text{max}}$ ) were used that were determined from the refinement of the standard material LaB<sub>6</sub> in PDFgui software.



# 5月15日閱讀研討會論文海報之照片

**OBJECTIVES**

- coordinated strategies
- facilities, methods, data
- within energy storage and
- other technologies
- open scientific, technological and
- ship in current and next generation
- technologies
- support for SET-Plan goals

**PARTICIPANTS**

15 member states, 470 participants

**Overall R&D OBJECTIVES**

- Improving energy density and storage efficiency
- Cost reduction, improving safety, reliability, availability, cycle life, calendar life, sustainability
- Standardization and quality issues, social acceptance, economic and environmental impacts

**CURRENT AND FUTURE ACTIVITIES**

- Review of activities, assessment of progress
- Identifying next step requirements and actions
- Coordinating research efforts
- Developing strategic roadmaps with the involvement of all stakeholders
- Identifying key research areas
- Establishing a joint research and innovation programme
- Identifying key research areas
- Establishing a joint research and innovation programme

**Nanoscale silicon as high capacity anode for next-generation lithium ion batteries**

Christoph Erk,<sup>1,2</sup> Torsten Brezesinski,<sup>1</sup> Heino Sommer,<sup>1,2</sup> Rihab Al-Salman,<sup>1</sup> Reinhard Schneider<sup>3</sup> and Jürgen Janek<sup>1,4</sup>

<sup>1</sup>Karlsruhe Institute of Technology, Eggenstein-Leopoldshafen, Germany; <sup>2</sup>BASF SE, Ludwigshafen, Germany; <sup>3</sup>Karlsruhe Institute of Technology, Karlsruhe, Germany; <sup>4</sup>Justus Liebig University Gießen, Gießen, Germany

**Introduction**

Silicon (Si) is a promising anode material for future lithium ion and next-generation lithium batteries. This is due in part to its natural abundance and high theoretical specific capacity of 4200 mAh/g when fully lithiated according to Li<sub>15</sub>Si<sub>4</sub>. However, accumulation of lithium is associated with large volume expansion of up to 300% and, thus, Si electrodes suffer from severe mechanical stress. As a result, they often fracture and pulverize after a few charge/discharge cycles.

Theoretically, a viable solution to this issue would be the use of nanoscale Si and SiC materials. However, many parameters, including electrolyte system, binder and so forth, are known to affect the cycling performance of Si electrodes. Therefore, optimization of a broad range of different "key" parameters is inevitable.

**Cycling behavior of Si-50 and Si-100 nanopowders**

| Rate       | Si-50 | Si-100 | EC   | EC:DMC |
|------------|-------|--------|------|--------|
| 1000 mAh/g | 1000  | 1000   | 1000 | 1000   |
| 500 mAh/g  | 1000  | 1000   | 1000 | 1000   |
| 200 mAh/g  | 1000  | 1000   | 1000 | 1000   |
| 100 mAh/g  | 1000  | 1000   | 1000 | 1000   |

**Results**

**Introduction**

Silicon (Si) is a promising anode material for future lithium ion and next-generation lithium batteries. This is due in part to its natural abundance and high theoretical specific capacity of 4200 mAh/g when fully lithiated according to Li<sub>15</sub>Si<sub>4</sub>. However, accumulation of lithium is associated with large volume expansion of up to 300% and, thus, Si electrodes suffer from severe mechanical stress. As a result, they often fracture and pulverize after a few charge/discharge cycles.

Theoretically, a viable solution to this issue would be the use of nanoscale Si and SiC materials. However, many parameters, including electrolyte system, binder and so forth, are known to affect the cycling performance of Si electrodes. Therefore, optimization of a broad range of different "key" parameters is inevitable.

**Cycling behavior of Si-50 and Si-100 nanopowders**

| Rate       | Si-50 | Si-100 | EC   | EC:DMC |
|------------|-------|--------|------|--------|
| 1000 mAh/g | 1000  | 1000   | 1000 | 1000   |
| 500 mAh/g  | 1000  | 1000   | 1000 | 1000   |
| 200 mAh/g  | 1000  | 1000   | 1000 | 1000   |
| 100 mAh/g  | 1000  | 1000   | 1000 | 1000   |

**Results**

**Effect of Binder and Electrolyte**

Generally, cells containing the micro-morphological graphite (FEC)-based electrolyte show better cycling behavior than that achieved using the ethylene carbonate (EC)-based electrolyte.

PAA binder reveals the best cycling performance followed by PAA, AA, PVDF and CMC.

**Effect of SiO<sub>2</sub> content**

Two types of Si nanopowders were used in this work: one with a narrow particle size distribution (Si-50) and the other with a broad particle size distribution (Si-100).

Si-50 has a higher theoretical specific capacity than Si-100.

Si-50 has a higher theoretical specific capacity than Si-100.

**Conclusions**

- Regardless of both polymer binder and active material, cells with FEC-based electrolyte show better cycling performance than those with EC-based electrolyte.
- PAA binder shows overall best performance followed by PAA, AA, PVDF and CMC binders.
- Silicon nanopowders with narrow size distribution and thin oxide shells favor more beneficial to achieve high specific capacities and low first cycle irreversibilities and to keep the micro-morphological stability to lithium ion.
- Positive buffering effects of oxide species on the cycling behavior are not observed.

**Introduction**

Silicon (Si) is a promising anode material for future lithium ion and next-generation lithium batteries. This is due in part to its natural abundance and high theoretical specific capacity of 4200 mAh/g when fully lithiated according to Li<sub>15</sub>Si<sub>4</sub>. However, accumulation of lithium is associated with large volume expansion of up to 300% and, thus, Si electrodes suffer from severe mechanical stress. As a result, they often fracture and pulverize after a few charge/discharge cycles.

Theoretically, a viable solution to this issue would be the use of nanoscale Si and SiC materials. However, many parameters, including electrolyte system, binder and so forth, are known to affect the cycling performance of Si electrodes. Therefore, optimization of a broad range of different "key" parameters is inevitable.

**Cycling behavior of Si-50 and Si-100 nanopowders**

| Rate       | Si-50 | Si-100 | EC   | EC:DMC |
|------------|-------|--------|------|--------|
| 1000 mAh/g | 1000  | 1000   | 1000 | 1000   |
| 500 mAh/g  | 1000  | 1000   | 1000 | 1000   |
| 200 mAh/g  | 1000  | 1000   | 1000 | 1000   |
| 100 mAh/g  | 1000  | 1000   | 1000 | 1000   |

**Results**

**Effect of Binder and Electrolyte**

Generally, cells containing the micro-morphological graphite (FEC)-based electrolyte show better cycling behavior than that achieved using the ethylene carbonate (EC)-based electrolyte.

PAA binder reveals the best cycling performance followed by PAA, AA, PVDF and CMC.

**Effect of SiO<sub>2</sub> content**

Two types of Si nanopowders were used in this work: one with a narrow particle size distribution (Si-50) and the other with a broad particle size distribution (Si-100).

Si-50 has a higher theoretical specific capacity than Si-100.

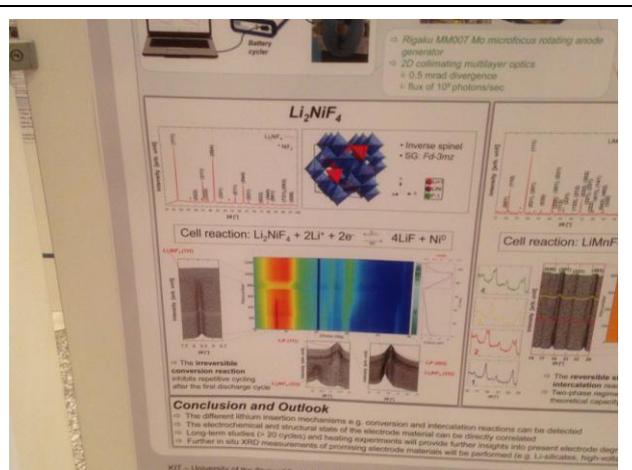
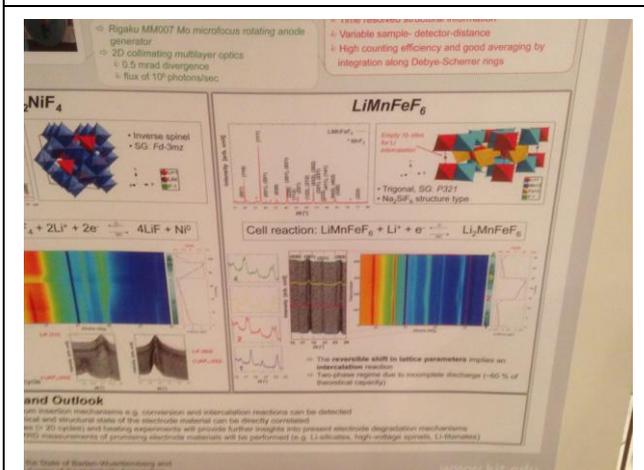
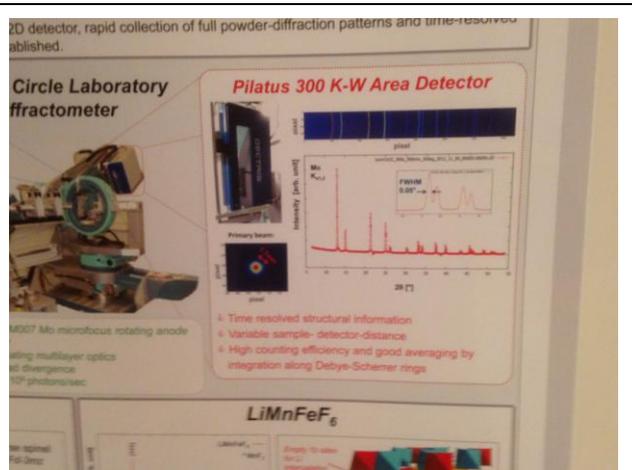
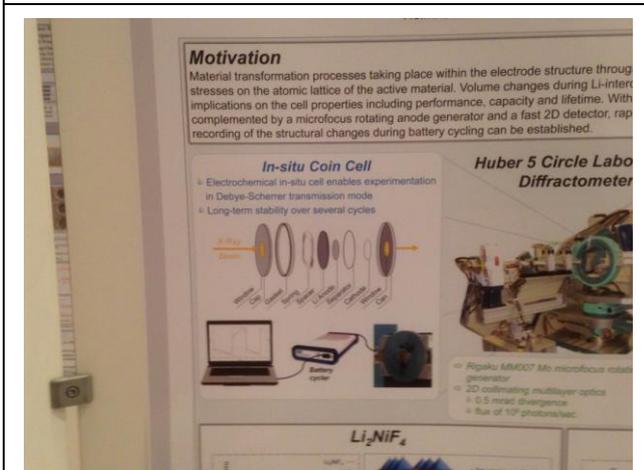
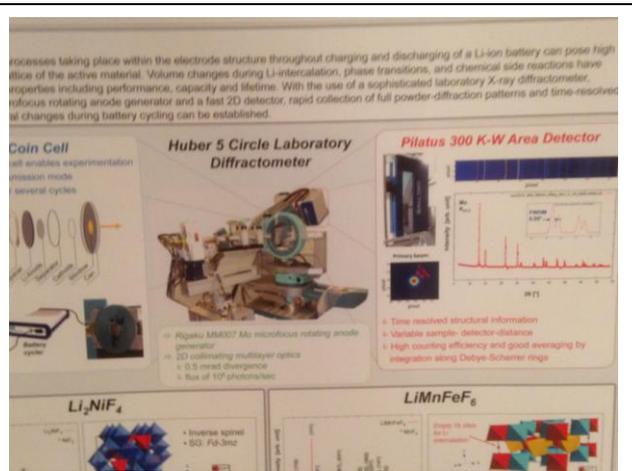
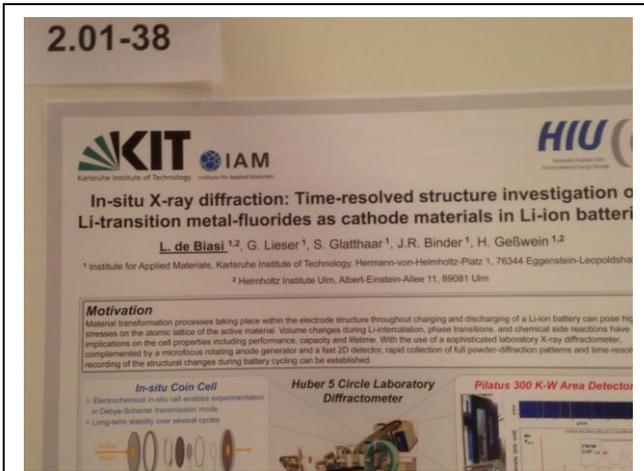
Si-50 has a higher theoretical specific capacity than Si-100.

**Conclusions**

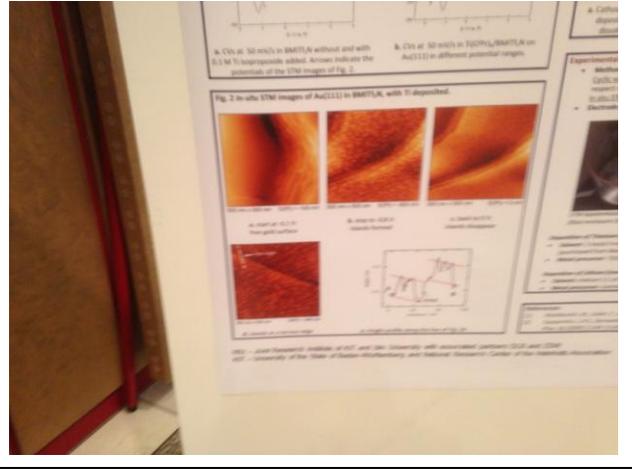
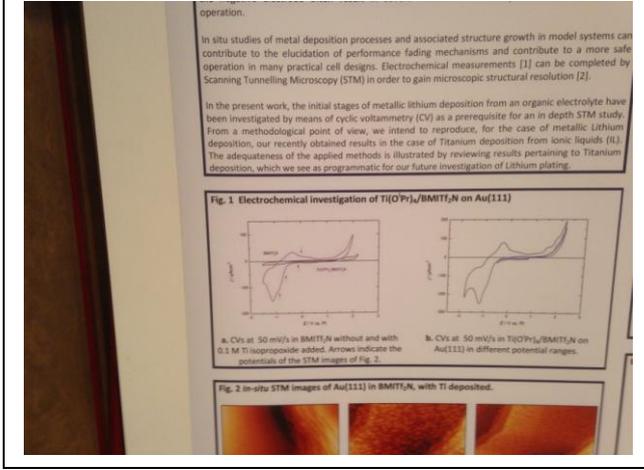
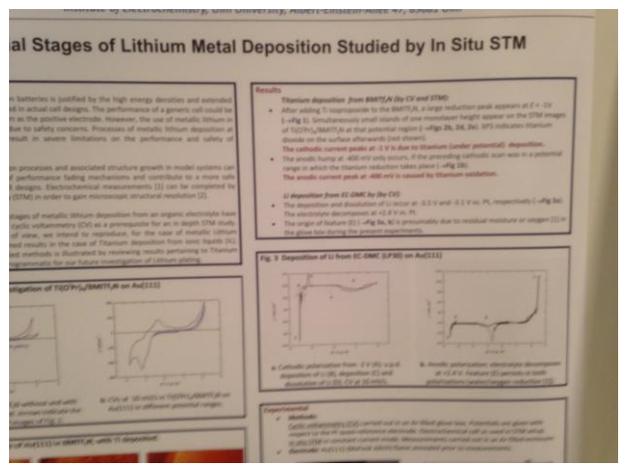
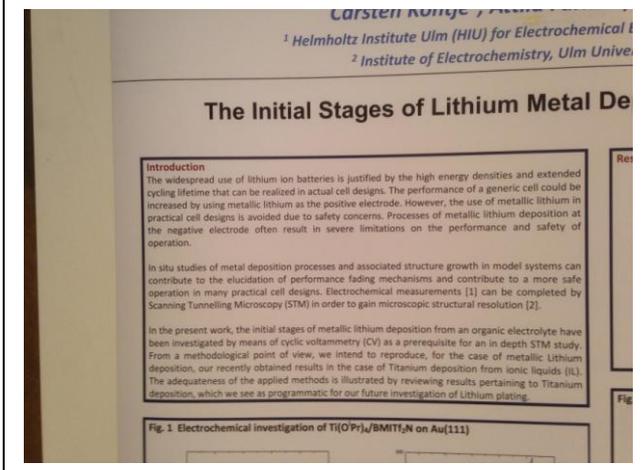
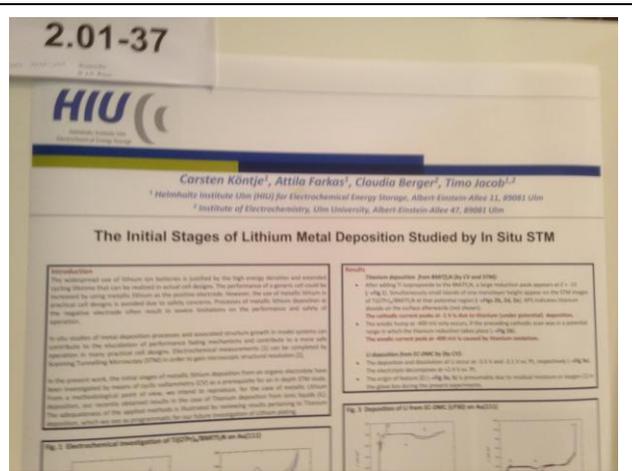
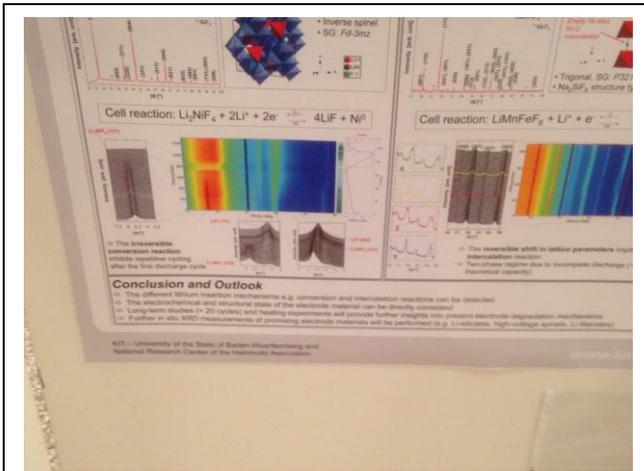
- Regardless of both polymer binder and active material, cells with FEC-based electrolyte show better cycling performance than those with EC-based electrolyte.
- PAA binder shows overall best performance followed by PAA, AA, PVDF and CMC binders.
- Silicon nanopowders with narrow size distribution and thin oxide shells favor more beneficial to achieve high specific capacities and low first cycle irreversibilities and to keep the micro-morphological stability to lithium ion.
- Positive buffering effects of oxide species on the cycling behavior are not observed.



# 5月16日閱讀研討會論文海報之照片



# 5月16日閱讀研討會論文海報之照片



附件三：大會函文邀請本人提供簡報資料



王強尼 <johnny.ic.wang@gmail.com>

---

## Materials for Energy 2013 conference - publication of your presentation

2 封郵件

---

**martz@dechema.de** <martz@dechema.de>

2013 年 5 月 23 日下午 4:56

收件者： johnny.ic.wang@gmail.com

Dear Prof. Wang

Thank you for your oral presentation at the Materials for Energy 2013 conference, titled:

Controlled oxide layer formation on corrosion behavior of Ti-6Al-4V alloy following thermohydrogen processing.

We would like to publish your presentation on a Web based platform and make it available for download for all participants of the conference. Therefore we kindly ask you to submit your presentation in pdf format electronically.

Please submit your electronic file via internet till May 30 at the latest at

<http://events.dechema.de/en/enmatsubmissionofpresentation> by using your submission number 3164.

All submitted presentations will be made available for download to all registered participants of the conference. You will be informed about the login access if available.

Best regards

Claudia Martz

DECHEMA e.V.

Congress Office EnMat II

Theodor-Heuss-Allee 25, 60486 Frankfurt am Main, Germany

Phone: +49 69-7564-129, Fax: +49 69-7564-176, E-Mail: [info@enmat.de](mailto:info@enmat.de), [www.dechema.de/enmat2013](http://www.dechema.de/enmat2013)

\*\*\*\*\*

Vorsitzender: Prof. Dr. Rainer Diercks, Schatzmeisterin: Almuth Poetz, Geschäftsführer: Prof. Dr. Kurt Wagemann

VR-Nr.: 73 VR 5293, Steuer-Nr.:045 250 52084, USt.-Id.-Nr.: DE 114234833